



**DI**  
**C**  
**Ma**  
**PI**

Dipartimento  
di Ingegneria Chimica,  
dei Materiali e della  
Produzione Industriale  
Università degli Studi  
di Napoli Federico II

Ph.D. in Chemical Engineering

(XXVIII Cycle)

**REGENERATION OF CATALYST-COATED  
DIESEL PARTICULATE FILTERS**

Thesis

**Supervisor**

Prof. Almerinda Di Benedetto

**Candidate**

Anna Saliva

**Scientific Committee**

Dr. Valeria Di Sarli (*Tutor*)

Prof. Debora Fino

Dr. Gianluca Landi

Dr. Luciana Lisi

Prof. Paola Russo

## Index

1. Introduction.....	3
2. State of the Art .....	8
2.1 Diesel Particulate Filters .....	8
2.2 The Mechanisms of Soot Oxidation .....	13
2.3 Catalysts for Diesel Particulate Filters .....	15
3. Aim of the Work .....	22
4. Approach .....	23
5. Experimental .....	24
5.1 Catalytic Filter Preparation .....	25
5.2 Catalytic Filter Characterization.....	29
5.3 Apparatus for Regeneration Tests.....	30
6. Results and Discussion .....	36
6.1. Regeneration Tests.....	36
6.1.1 Thermal Regeneration.....	36
6.1.2 Comparison between Thermal and Catalytic Regeneration.....	37
6.1.3 Colloidal Suspension of Ceria versus Solution of Cerium Nitrate .....	41
6.1.4 Effect of the Catalyst Morphology .....	43
6.2. Chemical and Physical characterization.....	46
6.2.1 Filter Characterization .....	46
6.3. Effect of the Catalyst/Soot Ratio .....	51
6.3.1 Effect of the Catalyst/Soot Ratio “with cake” .....	52
6.3.2 Effect of the Catalyst/Soot Ratio “without cake” .....	54
6.3.3 “Cake” versus “No cake” .....	55
7. Conclusions .....	65
Acknowledgements.....	67
Literature Cited.....	68

## 1. Introduction

Diesel engines are the workhorses for the modern society since they are widely used to transport goods, services and people. They also play a vital role in power generation and are used for farming, construction and industrial activities. Approximately 53% of new cars sold in Europe have diesel engines (European Automotive Manufacturer's Association, 2010), due to fact that diesel engines can offer efficiencies close to 45% and longer durability. But the diesel engine is one of the largest contributors to environmental pollution problems worldwide, and will remain so, with large increases expected in vehicle population causing ever-increasing global emissions of diesel particulate material (PM) and nitrogen oxides (NO<sub>x</sub>). Diesel exhaust differs from petrol engine exhaust in two major characteristics. Firstly, diesel exhaust contains a far higher amount of particulate matter and NO<sub>x</sub>, and secondly, the exhaust is far leaner, that is, far less unburned hydrocarbons and carbon monoxide than a typical exhaust from petrol engines.

Diesel PM consists mostly of carbonaceous soot with minor components of volatile organic fraction (VOF), unburned fuel and lubricating oil (soluble organic fraction, SOF) and inorganic compounds such as ash and sulphur compounds [Prasad and Bella, 2010].

Inside an engine, the complete combustion of the motor fuel composed exclusively of carbon and hydrogen would only generate CO<sub>2</sub> and H<sub>2</sub>O, to the exclusion of any other harmful product. However, the very short time allowed for chemical oxidation processes integration in combustion chambers, the lack of homogeneity in the fuel mixtures, and the heterogeneity and rapid variations in the temperature do not allow for the state of ideal thermodynamic

equilibrium to be reached. Thus, the incomplete combustion of a hydrocarbon results in the formation of a wide range of organic and inorganic compounds distributed among the gaseous, semi-volatile and particulate phases as shown in Table 1 [from Prasad and Bella, 2010]. The gaseous phase contains CO, CO<sub>2</sub>, NO<sub>x</sub>, SO<sub>x</sub>, NH<sub>3</sub>, water vapor, volatile organic compounds (VOC), hydrocarbons (HC), polycyclic aromatic hydrocarbons (PAH), organic/inorganic acids, halogenated organic compounds, dioxins, etc..

**Table 1. Typical diesel exhaust composition (from Prasad and Bella, 2010).**

Component	Concentration
CO	100-10000 ppm
HC	50-500 ppm, C <sub>1</sub>
NO <sub>x</sub>	30-1000 ppm
SO <sub>x</sub>	Proportional to fuel S content
DPM	20-200mg/m <sup>3</sup>
CO <sub>2</sub>	2-12 vol%
Ammonia	2.0 mg/mile
Cyanides	1.0 mg/mile
Benzene	6.0 mg/mile
Toluene	2.0 mg/mile
PAH	0.3 mg/mile
Aldehydes	0.0 mg/mile

Particles may be classified as primary or secondary depending on their formation mechanism. Primary particles are directly emitted into the atmosphere through diesel exhaust. Secondary particles are formed usually by chemical reactions of gaseous pollutants, such as sulphur oxides and nitrogen oxides interacting with other compounds in the air to form fine particles.

PM particles can be categorized in the following four sizes:

- Large particles, > 10  $\mu\text{m}$ ;
- Coarse particles, 2.5-10  $\mu\text{m}$  (PM10);
- Fine particles, 1.0-2.5  $\mu\text{m}$  (PM2.5);
- Ultra-fine particles, < 1.0  $\mu\text{m}$  (PM1.0).

The size of the particles also determines the time that they spend in the atmosphere. While sedimentation and precipitation removes PM10 from the atmosphere within few hours of emission, PM2.5 may remain there for days or even a few weeks. Consequently, these particles can be transported over long distances. More than 90% of diesel exhaust-derived PM is smaller than 1  $\mu\text{m}$  in diameter. Most of the mass is in the 0.1-1.0  $\mu\text{m}$  “accumulation” size

fraction, while most of the particles are in the  $< 0.1 \mu\text{m}$  “nano-particle” fraction. These small particles are respirable and penetrate deep into the lungs where they are able to enter the bloodstream and even reach the brain [Prasad and Bella, 2010]. Figure 1 shows the transport of the PM with breath according to the particle size [from Prasad and Bella, 2010].

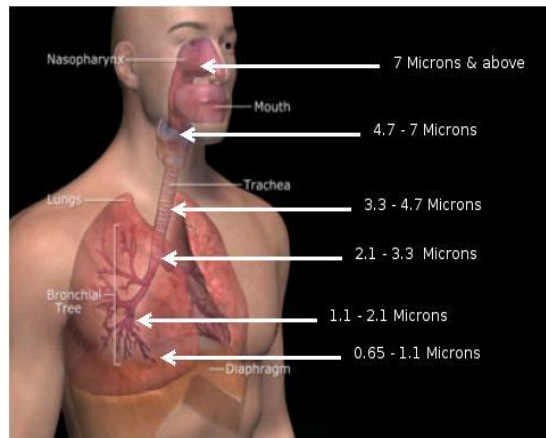


**Figure 1. Transport of the PM with breath according to the particle size (from Prasad and Bella, 2010).**

Diesel emissions are responsible for a lot of damage to human health resulting from simple irritations and allergies to more serious illnesses (such as cancer) and to genetic defects that can lead to infant death. In addition, the terrible effect of PM is also reflected in animals and the ecosystem with contamination of water and soil. The soot settling on glaciers or ice in arctic region absorbs solar heat directly and contribute to causing glaciers or ice to melt. This can lead flooding, rise in water level of sea. The atmospheric solar heating by soot, next to carbon dioxide, is the major contributor to global warming. The diesel engine is the most efficient internal combustion engine and its use is widely expanding. Unfortunately, diesel engines emit about 10 times more particulate matter (PM) than gasoline engines. Particle

emissions of road vehicles are subjected to restrictions in terms of mass per unit energy or travel. Government legislations for permissible exhaust emission standards were first introduced in both Europe and the United States of America in 1982 only for light-duty vehicles, and in 1990 also for heavy-duty engines. Table 2 shows the European standards for diesel emissions. All vehicles equipped with a diesel engine will be required to substantially reduce their emissions of nitrogen oxides (0.08 g/km) because the Euro VI standard was entered into force (1st September 2014) (the legislation of the European Union, 20th June 2007, available at [www.europa.eu/legislation\\_summaries/environment/air\\_pollution/l28186\\_en.htm](http://www.europa.eu/legislation_summaries/environment/air_pollution/l28186_en.htm)).

**Table 2. European standards for diesel vehicle emissions.**

Year	Reference	Light duty diesel (g/km)		Heavy duty diesel (g/kWh)	
		NO <sub>x</sub>	DPM	NO <sub>x</sub>	DPM
2000	Euro I India 2000	-	0.14-0.25	8.0	0.36
2005	Euro II Bharat	-	0.08-0.17	7.0	0.15
2008	Euro III Bharat	0.50-0.78	0.05-0.10	5.0	0.10
2010	Euro IV Bharat	0.25-0.33	0.025-0.04	3.5	0.02
2011	Euro V	0.18-0.235	0.005	0.235-0.28 (g/km)	0.005 (g/km)
2014	Euro VI	0.08	0.005	0.08 (g/km)	0.005 (g/km)

## 2. State of the Art

### 2.1 Diesel Particulate Filters

Legislations on diesel emissions have become over time more and more stringent and this has meant that the diesel particulate filter (DPF) has become the most important and complex device for emission control. A DPF is the most efficient device for PM removal from the engine effluents [Johnson, 2003]. Typically, it consists of thousands of square parallel ceramic channels, with the opposite ends of adjacent channels being plugged (“wall-flow” type filter, Figure 2).

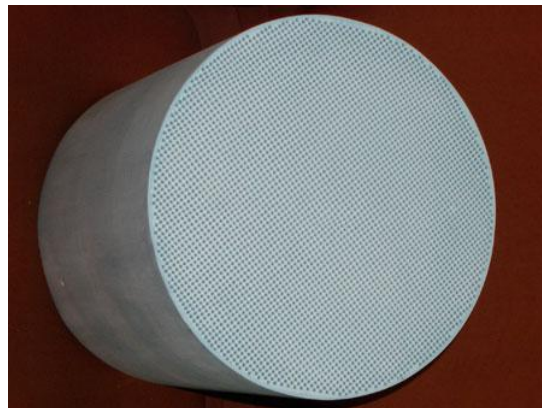


**Figure 2. Commercial wall-flow DPF (download of the image from [www.highpowermedia.com/ret-monitor/2947/diesel-particulate-filters](http://www.highpowermedia.com/ret-monitor/2947/diesel-particulate-filters)).**

Figure 3 shows a schematic of the flow in a channel of a wall-flow DPF [from Prasad and Bella, 2010]. The exhaust gases pass through the filter walls, the particulate matter is retained and cleaned exhaust gases are emitted.

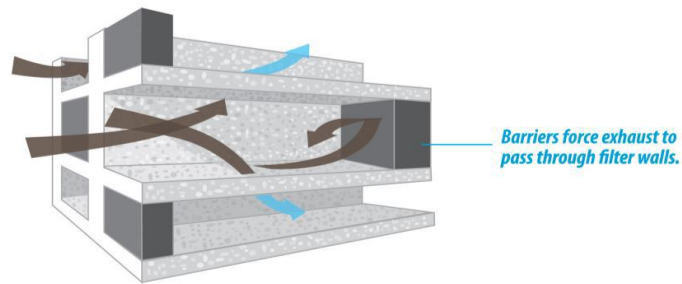


**Figure 3. Schematic representation of the flow in a channel of a wall-flow DPF (from Prasad and Bella, 2010).**

The mechanisms of interception of the PM particles can be classified as follows [Konstandopoulos and Papaioannou, 2008]:

- deep bed filtration - the particles of smaller size than the porous elements of the filter are deposited inside the filter material through the action of different fields of forces;
- cake filtration - the particles of larger size than the porous filter elements are deposited on the wall of the filter element being mechanically locked.

The progressive deposition of particles into the porous filter walls (deep bed filtration) and the formation of a superficial PM layer (cake filtration) modify both the filtration efficiency and the spatial distribution of PM inside the filter [Bensaid et al., 2009]. The deep bed filtration occurs in the initial phase and is characterized by a non-linear increase of the pressure drop,  $\Delta P$ , with the mass of accumulated PM. Conversely, the subsequent growth of the PM layer (cake) on the filter is characterized by a linear trend. Figure 4 shows the typical trend of  $\Delta P$  as a function of the mass of PM (i.e., soot) accumulated during filtration [from Konstandopoulos and Papaioannou, 2008]. Excessive values of  $\Delta P$  are an index of excessive

accumulation of PM, while low  $\Delta P$  values indicate the loss of mechanical integrity of the filter (it does not filter anymore).

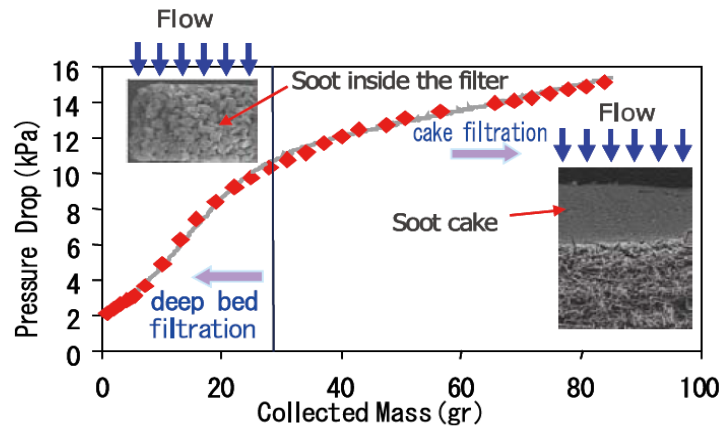


**Figure 4. Typical trend of pressure drop as a function of the mass of PM (i.e., soot) accumulated during filtration; two filtration modes can be distinguished, deep bed filtration and cake filtration (from Konstandopoulos and Papaioannou, 2008).**

The porous media of the traps can be either of ceramic material or of metallic material. The ceramic supports are:

- cordierite (extruded);
- mullite (extruded, foams, fibers);
- silicon carbide (extruded, foams, fabrics);
- tialite (extruded);
- mullite/zirconia (extruded, foams);
- mullite/tialite (extruded, foams);

while the metallic materials are:

- sintered metals;
- wire meshes;
- metal foams.

Wall-flow (extruded) filters are very efficient (> 90%) since they act as “cake filters”, whereas foams and fibers are somehow less efficient as a consequence of the deep bed filtration mechanism they enable [Fino, 2007]. PM accumulates on the walls of the DPF, affecting the engine performance and fuel efficiency [Schmidt et al., 2007]. To maintain the operational efficiency of the DPF, it is important to periodically remove the PM. The process that allows to perform this task is called “regeneration”. During regeneration, the PM accumulated on the filter is removed by combustion, leaving only small amounts of ash. An attractive way to regenerate the filter lies in the use of catalysts to enhance the combustion rate of the soot by reducing its ignition temperature. However, even in the presence of catalysts, the process of regeneration remains particularly critical as the exothermic combustion sometimes leads to excessive local temperature excursions that damage the filter [van Setten et al., 2001]. Figure 5 shows an example of massive melting on the downstream face of a DPF [from Martirosyan et al., 2010].

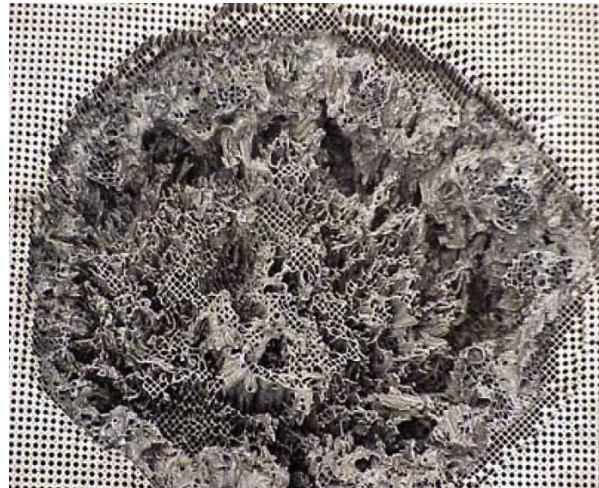


**Figure 5. Example of massive melting on the downstream face of a DPF (from Martirosyan et al., 2010).**

The different types of traps and their efficiencies, advantages and drawbacks are summarized in Table 3 [from Rocco, 2009].

**Table 3. Types of traps and their efficiencies, advantages and drawbacks (from Rocco, 2009).**

Type of trap	Efficiency %	Advantages	Drawbacks
Ceramic monolith	60 – 95	<ul style="list-style-type: none"> <li>• High efficiency</li> <li>• Moderate cost</li> <li>• Can be covered with catalyst</li> </ul>	<ul style="list-style-type: none"> <li>• Moderate <math>\Delta P</math></li> <li>• High <math>\Delta P</math> gradient</li> <li>• Subject to thermal shock cracking</li> </ul>
Aluminated metallic sponge (precious metal catalyst)	50 – 80	<ul style="list-style-type: none"> <li>• Low <math>\Delta P</math> gradient</li> <li>• Self regenerable</li> <li>• Reduces (HC, CO and odor)</li> </ul>	<ul style="list-style-type: none"> <li>• Moderate <math>\Delta P</math></li> <li>• Low efficiency especially at high speed</li> <li>• Produce sulfates</li> </ul>
Ceramic foam	30 – 75	<ul style="list-style-type: none"> <li>• Good thermal shock resistance</li> <li>• Can be covered with catalyst</li> </ul>	<ul style="list-style-type: none"> <li>• Regeneration difficult</li> <li>• Very high <math>\Delta P</math></li> <li>• Low efficiency</li> </ul>
Ceramic fiber sponge	>75	<ul style="list-style-type: none"> <li>• Very high efficiency</li> <li>• Good thermal shock resistance</li> </ul>	<ul style="list-style-type: none"> <li>• Fiber disintegration</li> <li>• High <math>\Delta P</math> gradient</li> <li>• Large volume and weight</li> </ul>
Woven silica fiber coil filter	>75	<ul style="list-style-type: none"> <li>• Good thermal shock resistance</li> <li>• Low <math>\Delta P</math></li> <li>• High efficiency</li> </ul>	<ul style="list-style-type: none"> <li>• Large volume demand</li> </ul>

The materials used in the monolith filters that equip the cars currently on the market are the cordierite (traditional material) and the silicon carbide (more recent material). The silicon carbide has greater resistance to high temperature, but higher weight and cost.

## 2.2 The Mechanisms of Soot Oxidation

The mechanisms of soot oxidation that play an important role in the regeneration of the filters can be classified as follows [DieselNet, 2005]:

- Oxidation by  $O_2$ ;
- Oxidation by  $NO_2$ ;
- Thermal oxidation by  $O_2$ .

Oxidation by  $O_2$  is characterized by the fact that the soot particles are oxidized by the oxygen adsorbed on the catalytic sites. This mechanism is limited to particles that physically come into contact with the catalytic sites. Oxidation by  $NO_2$  can be generated by the catalytic oxidation of NO. Catalytic oxidation of hydrocarbons and other gas species, as well as carbon particulates themselves, can create local zones of increased temperature due to the exothermal heat of reaction. The increased temperature may be sufficient ( $> 600^\circ C$ ) to activate (non-catalytic) thermal oxidation of soot deposits.

$O_2$  is left out from the air in excess of the combustion process and its concentration is about 10%. NO is formed at high temperature and pressure from  $N_2$  and  $O_2$  present in the air in excess during combustion.  $NO_2$  is formed by reaction of NO with  $O_2$  in excess. The

concentration of nitrogen oxides in the emissions is about 0.01-0.1%, 2-3 orders of magnitude lower than that of O<sub>2</sub>. 90-95% of NO leave the engine such as NO and only 5-10% as NO<sub>2</sub>. NO<sub>2</sub> oxidizes the soot to CO<sub>2</sub> with reasonable speed in the temperature range 50-300°C [Görsmann, 2005].

Figure 6 shows an example of soot (i.e., carbon) oxidation rate by O<sub>2</sub> and NO<sub>2</sub> versus temperature with and without catalyst [DieselNet, 2005].

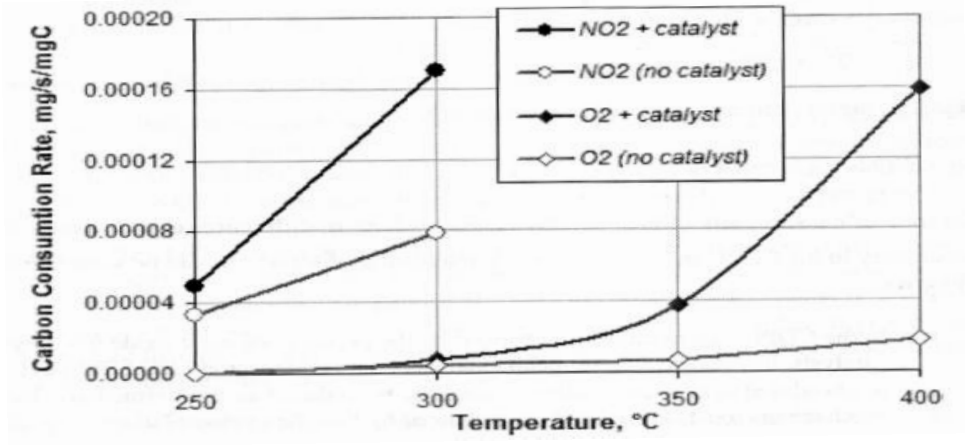


Figure 6. Carbon oxidation rate by O<sub>2</sub> and NO<sub>2</sub> versus temperature with and without catalyst (from DieselNet, 2005).

## 2.3 Catalysts for Diesel Particulate Filters

Catalytic regeneration of diesel particulate filters (DPFs) has been proposed as an alternative or complementary approach to bypass or mitigate the drawbacks associated with thermal regeneration (additional energy costs, complex means of control, local temperature excursions sufficiently high to damage the DPF, CO & CO<sub>2</sub> formation etc.) [Fino and Specchia, 2008; Fino et al., 2016; Koltsakis et al, 2007]. In principle, the catalyst may be used to achieve soot oxidation at temperatures lower (250-550°C) than those required for thermal regeneration (> 600°C), and/or to shorten the regeneration time period, thus allowing for energy saving.

From the filtration point of view, the main problem of catalytic (i.e., catalyst-coated) DPFs (CDPFs) is the increase in pressure drop as compared to the bare filter, due to the additional resistance to the gas flow opposed by the wash-coat layer located on top of the porous wall of the filter [Kumar et al., 2012]. However, this problem can be overcome and, thus, the filtration properties preserved, utilizing the porous wall of the DPF substrate, with its large total volume, as support for a thin catalytic layer without causing major changes in pore size distribution [Guan et al., 2015]. In fact, in this work the use of a particular active catalyst whose dimensions, as well as optimal loading suitably chosen makes possible the deposition of the catalyst within the macroporous structure of the filter without leading significant changes to the initial porosimetric distribution of the filter. In this way on the one hand the increase in pressure drop can be avoided preserving the filtering properties and on the other hand the contact between the deposited catalyst and the collected soot is maximized .

From the regeneration point of view, there is still no general consensus regarding the ability of CDPFs to oxidize soot at low temperatures and under conditions relevant to practical applications [Southward et al., 2010]. Indeed, such ability is strictly dependent not only on the intrinsic catalyst activity, but also on the efficiency of the contact between the soot particles and the active sites of the catalyst particles [van Setten et al., 2000; Hinot et al., 2007].

Therefore the soot-catalyst contact is a key element for soot oxidation [Fino et al., 2003]. Some catalytic elements are mobile enough under reaction conditions to “wet” the soot surface and effectively disperse their activity and move to non-reacted soot. Other catalysts remain as discrete particles but are mobile enough to maintain contact with the soot. More static catalytic elements require the soot to contact them [van Setten et al., 2000]. There are different ways to compensate for the low mobility of soot during its catalytic combustion. One way is to oxidize with a catalyst all NO present in the exhaust to NO<sub>2</sub> which, was discussed in Sub-section 2.2, is very reactive with soot and burns it at relatively low temperatures. The other way is to create large contact area between the catalyst and the soot, so that the soot can be directly burned with O<sub>2</sub> [van Setten et al., 1999].

The catalysts used in diesel particulate filters are divided into two categories:

- Platinum group metals (PGM) catalysts;
- PGM-free catalysts.

PGM catalysts include Pt and other metals of the same group (such as Pd, Rh and Ru). The most commercial and most active noble metal based filter uses Pt, usually combined with promoters, known to be active to oxidize CO and HC. Pt is expensive. In addition, it forms sulfate particulates (therefore, its application is limited when using fuels containing high S contamination) and/or NO<sub>x</sub> emissions [DieselNet, 2005].

PGM catalysts are very active for the soot oxidation reaction [Cooper and Thoss, 1989; Neri et al., 1997]. Cooper and Thoss [1989] observed and reported Pt promoting soot oxidation indirectly. The combustion mechanism involves a two-step process in which the NO present in exhaust gas is converted into the active oxidant NO<sub>2</sub> over the Pt catalyst. This NO<sub>2</sub> subsequently oxidizes soot at a faster rate than oxygen.

Neri et al. [1997] observed high activity of Pt supported on  $\gamma$ -Al<sub>2</sub>O<sub>3</sub> in air, even at low loadings of the noble metal. Spillover of activated oxygen from Pt to the support was postulated to take into account the promotion of soot oxidation.

Pt features high activity for oxidation of SO<sub>2</sub> to H<sub>2</sub>SO<sub>4</sub>, which is a drawback. The addition of Rh to Pt effectively reduces the SO<sub>2</sub> oxidation to SO<sub>3</sub> [Dettling and Skomoroski, 1992], but significantly increases the filter regeneration temperature [Uchisawa et al., 1998].

The effect of Pt supported catalysts on soot oxidation was intensively studied by Uchisawa et al. [2001]. Numerous support metal oxides [Uchisawa et al., 2003a] were impregnated with different Pt precursors [Uchisawa et al., 2003b] to determine the catalytic activity. Pt(NH<sub>3</sub>)<sub>4</sub>(OH)<sub>2</sub>/MO<sub>x</sub>/SiC (MO<sub>x</sub> = TiO<sub>2</sub>, ZrO<sub>2</sub> and Al<sub>2</sub>O<sub>3</sub>) showed relatively high oxidation

activity and durability at high temperatures and with exposure to sulfate. The authors suggested that the supports with low basicity reduce the affinity toward  $\text{SO}_3$ .

V is known to reduce the sulphate in diesel oxidation catalysts. The effect of V on Pt based catalysts for the reduction of diesel emissions was studied under  $\text{SO}_2$  conditions by Liu et al. [2001] and Kim et al. [2003].

As reviewed by Prasad and Bella [2010], various catalyst systems based on transition metal oxides/salts (Co-Ni, Cu-Fe, K-Cu, K-Co, Co-Ba-K, Cu-K-Mo, Cu-V-K, Cs-Fe-V) and rare earth metal oxides (Ce-La, La-Cr, Pr-Cr, La-K, La-K-Cr, La-K-Mn-O, La-K-Cu-V and Co-Ce) have been studied and demonstrated the promise for diesel exhaust treatment. These non-noble metal catalysts (i.e., PGM-free catalysts) are less expensive and generally less reactive than PGM catalysts. They also exhibit lower activity in the oxidation of CO and HC, but form little or no sulfate particulates and/or  $\text{NO}_x$  emissions [DieselNet, 2005].

Watabe et al. [1986] was the first to report a catalyst based on a formulation of Cu/K/M/(Cl), where M is V or Mo. For years, catalysts based on this formulation were investigated extensively [see, e.g., Ciambelli et al., 1999] because they exhibit high soot oxidation rates at low temperatures. The high activity was related to the mobility and volatility of the active copper chloride component of the catalyst [Mul et al., 1997]. Unfortunately, catalyst compounds evaporate during soot oxidation, making the feasibility of the catalyst questionable.

Various alternatives for the Cu/K/M/(Cl) formulation have been investigated. Querini et al. [1998] compared Co/MgO and Co/K/MgO catalysts and concluded that the enhanced

catalyst mobility induced by potassium increases activity. Badini et al. [1998] reported that K-V-I containing catalysts are active catalysts, but they also reported the emission of volatile components of the catalysts. Ahlström and Odenbrand [1990] reported mobile catalysts that did not evaporate during soot oxidation.

More recently, the research group of Prof. Trovarelli (University of Udine) intensively studied CeO<sub>2</sub> based formulations for soot oxidation [Aneghi et al., 2007; 2009; 2012]. In particular, Aneghi et al. [2009] proposed a Ag-doped CeO<sub>2</sub> catalyst that, with a combustion temperature of 330°C, can be included, at present, among the most promising catalysts. Moreover, CeO<sub>2</sub> based catalysts show synergetic effect in the oxidation of soot with NO and O<sub>2</sub> [Atribak et al., 2009] and for these reasons represent a class of materials worth of investigation for soot combustion assisted by NO<sub>x</sub>.

The new stringent regulation limits (Euro VI) on soot and NO<sub>x</sub> emissions are forcing to develop innovative multifunctional catalytic systems that combine denitrification catalysts with catalytic filters.

Li et al. [2010] prepared Fe-substituted nanometric perovskite-type catalysts (La<sub>0.9</sub>K<sub>0.1</sub>Co<sub>1-x</sub>Fe<sub>x</sub>O<sub>3-δ</sub>) showing highest activity at  $x = 0.1$  for simultaneous removal of soot and NO<sub>x</sub>. However, over the proposed catalyst, the maximal soot oxidation rate was achieved at only 362°C. In any case, ceria (alone or in combination with other oxides) is among the most active catalysts for soot oxidation due to its redox properties (Ce<sup>4+</sup>/Ce<sup>3+</sup>) and oxygen storage capacity [Trovarelli and Fornasiero, 2013; Bueno-López, 2014]. Furthermore, the low cost (as compared to noble metals) makes ceria-based materials particularly attractive. In order to

increase the number of soot-catalyst contact points, thus favoring the solid-solid interaction, ceria-based catalysts with engineered morphologies, such as fibers, sticks, flakes, cubes, rods and stars, have been proposed [Kumar et al., 2012; Bensaid et al., 2013, Piumetti et al., 2015]. Bensaid et al. [2013] compared fibers, sticks and flakes, showing that the fibrous morphology is the best one for soot oxidation, probably due to the network of fibers which surround the soot particles, thus maximizing the number of contact points. On the other hand, the self-assembled stars synthesized by Miceli et al. [2015], so-called due to their branched morphology characterized by individual rods assembled in three-dimensional star-shaped way starting from a central nucleus, also exhibit a high availability of contact points between the soot particles and the catalyst itself, each rod offering a concave space for soot intrusion.

Among the mechanisms of oxidation discussed in Sub-section 2.2, in particular two mechanisms of ceria-catalyzed soot combustion have been identified: the oxidation by  $O_2$ , the so-called “active oxygen” mechanism, and the oxidation by  $NO_2$ , the “ $NO_2$ -assisted” mechanism [Bueno-López, 2014]. These two mechanisms may occur simultaneously in soot/ $O_2$ /NO reaction.

In the “active oxygen” mechanism, the exchange of oxygen atoms between the ceria catalyst and the O-containing gases ( $O_2$  is the most abundant one in a diesel exhaust) produces highly reactive oxygen species at the catalyst surface (the so-called “active oxygen”), which can oxidize soot very efficiently. However, active oxygen species must be transferred from the ceria catalyst to the soot particles (i.e., to the soot-catalyst interface), before they recombine with each other to form  $O_2$ . This transfer process, which occurs by superficial diffusion,

makes the soot-ceria contact a key issue for an efficient soot combustion. Once surface oxygen-carbon complexes are formed upon  $O_2$  oxidation, they decompose and yield  $CO/CO_2$ , whereas the free carbon sites created on the surface become available to chemisorb further oxidizing molecules.

In the “ $NO_2$ -assisted” mechanism, the ceria catalyst catalyzes  $NO$  oxidization to  $NO_2$ , which is more reactive than  $O_2$  and, as such, can initiate soot combustion. Once  $NO_2$  reacts with soot, the remaining part of the mechanism is similar to that described for “active oxygen”.

All the proposed engineered morphologies have been successfully tested in powdered soot-catalyst mixtures and, thus, under conditions of soot-catalyst contact that, even in the case of the “loose” contact conditions (e.g., soot and catalyst mixed with a spatula), which are more realistic testing conditions than the “tight” contact ones (e.g., soot and catalyst mixed in a mortar) [van Setten et al., 2000], are quite far from those actually established during filter regeneration.

### 3. Aim of the Work

In this work, *the optimization of the soot catalyst-contact* was investigated. In literature all the proposed engineered morphologies have been successfully tested in powdered soot-catalyst mixtures and, thus, under conditions of soot-catalyst contact which are quite far from those actually established during filter regeneration. Conversely, in this work, the effect of the presence of the catalyst on the soot oxidation in a *diesel particulate filter (DPF)* was tested. The diesel particulate filter (DPF) with *ceria* was wash-coated. The catalyst load was suitably chosen to *avoid major changes in pore size distribution* of the original filter *preserving the filtering properties*. In addition *the link between regeneration performance and soot-catalyst distribution was quantified*.

## 4. Approach

Filters cut from commercial silicon carbide (SiC) DPFs and wash-coated with (the same amount of) ceria were loaded with different amounts of soot, thus varying the catalyst/soot ratio. Filter samples were characterized by N<sub>2</sub> physisorption at 77 K, Hg intrusion porosimetry and SEM/EDX analysis to study the modification in pore structure and morphology of the original commercial filter upon CeO<sub>2</sub> coating and/or soot deposition. Regeneration tests were performed in a lab-scale plant by temperature programmed combustion of soot under an O<sub>2</sub>/N<sub>2</sub> atmosphere. Thus, the role of ceria in this study is to catalyze the direct combustion of the soot particles trapped inside the filter and not to catalyze the oxidation of NO to NO<sub>2</sub>.

Definitely the study of the regeneration of catalyst-coated diesel particulate filters was performed through the following three steps:

1. Preparation of the filter;
2. Chemico-physical characterization of the catalytic (lab-scale) filter;
3. Tests of the regeneration dynamics of the catalytic (lab-scale) filter.

## 5. Experimental

The experimental activity was performed within the Laboratory of Catalysis of the Institute for Research on Combustion of the National Research Council (IRC-CNR). The following action steps have been taken:

1. Catalytic filter preparation;
2. Catalytic filter characterization;
3. Regeneration tests.

## 5.1 Catalytic Filter Preparation

The filters were obtained starting from a commercial silicon carbide (SiC) filter (quadratic prism with side length = 3.4 cm and axial length = 15 cm; 180 cpsi; porosity = 0.42) provided by IBIDEN. Each filter was cut several times along both longitudinal and transverse directions to obtain monoliths having an axial length of 3-3.2 cm and a square section with side length of 1.3 cm. One channel was eliminated from each corner, thus obtaining monoliths with a pseudo-cylindrical shape.

During the cutting operation, the original plugs of the IBIDEN filter were lost. Thus, to plug the opposite ends of adjacent channels of the monolith (thus recovering the original filter configuration), a ceramic paste was used. The paste was obtained from a SiC powder and a liquid activator (22-26 parts of activator per 100 parts of silicon carbide) (Rescor Castable Ceramics, 770, COTRONICS CORP.). Each base of the monolith was filled with the ceramic paste by using a spatula and, then, alternate channels were unplugged by using a needle. The small filters were left at room temperature for about 24 hours. Then, they were calcined at 950°C for 5 hours (heating rate of 1°C/min). Each filter was rinsed in bi-distilled water (to eliminate the residual ceramic paste) and then left to dry in an oven at 100°C for about 30 minutes.

The filter was catalyst-coated and soot-loaded. The catalyst was ceria ( $\text{CeO}_2$ ) obtained starting from a colloidal suspension (NYACOL,  $\text{CeO}_2$  (AC)) consisting of nano-sized ceria particles dispersed in a solution of acetic acid (particle size: 10-20 nm). The filter was dipped for 5 minutes in 50 ml of colloidal suspension and, then, rotated 180 degrees and dipped for

further 5 minutes. After dipping, the filter was vigorously shaken, to eliminate the excess material, and placed in an oven at 100°C for 40 minutes (to allow uniform drying, it was rotated every 10 minutes). To obtain the active catalytic phase, the filter was calcined at 450°C for 2 hours (heating rate of 10°C/min). The cycle of dipping, shaking, drying and calcination was repeated three times to achieve the desired target (~ 1 g). Alternatively to the colloidal suspension, a solution of a cerium nitrate (Cerium (III) nitrate hexahydrate, FLUKA) was used. The solution consisted of 5 g of cerium nitrate in 100 ml of bi-distilled water. The same steps were followed as described for the colloidal ceria. In addition ceria in form of nanocubes and stars was obtained. CeO<sub>2</sub> in form of nanocubes was synthesized through the hydrothermal procedure. NaOH (24 g) and Ce(NO<sub>3</sub>)<sub>3</sub> · 6H<sub>2</sub>O (2.2 g) were dissolved in 35 mL and 5 mL of bi-distilled water, respectively. Then the two solutions were mixed together and stirred for 1 h, which resulted in the formation of a milky slurry. After that the final mixture was transferred to an autoclave (150 mL) which was 75% filled with deionised water. Then the mixture was aged at 165°C (to form nanocubes) for 24 h so the fresh precipitates were separated by centrifugation, washed with deionised water several times, washed in ethanol and dried at 60°C overnight. In the end the powders were calcined at 550°C in synthetic air for 4 h. While CeO<sub>2</sub> in form of stars was prepared by hydrothermal synthesis in a stirred batch reactor, dropping 100 ml of a 0.2 M of cerium (III) chloride heptahydrate in 100 ml of a 0.01 M CTAB (Cetyl trimethylammonium bromide) aqueous solution adding 80 mmol of solid urea (corresponding to a 4:1 molar ratio between urea and the cerium salt). After 24 h at 120°C, a white precipitate was obtained then dried at 60°C for 24 h and calcined at 600°C for 4 h.

After the catalyst-coating, the filter was loaded with soot. To this end, the technique described in van Setten et al. [1999] was adopted. In particular, 1 g of soot (Degussa Printex U) was dispersed in 100 ml of heptane (Sigma Aldrich). Each filter was “hanged” through a thin copper wire to be dipped in the suspension and, then, rotated 180 degrees and immersed again. The time duration of the dipping phase and the number of re-petitions of the whole procedure were varied to vary the soot load and, thus, the catalyst/soot ratio. After dipping, the filter was vigorously shaken and, then, dried for 1 h at room temperature (to allow the heptane evaporation).

To ensure homogeneity of the colloidal suspension and, mainly, of the suspension of soot in heptane, both suspensions were magnetically stirred.

Figure 7 shows the monoliths after the stages of cutting, plugging, catalyst-coating and soot-loading (along with the original IBIDEN filter).

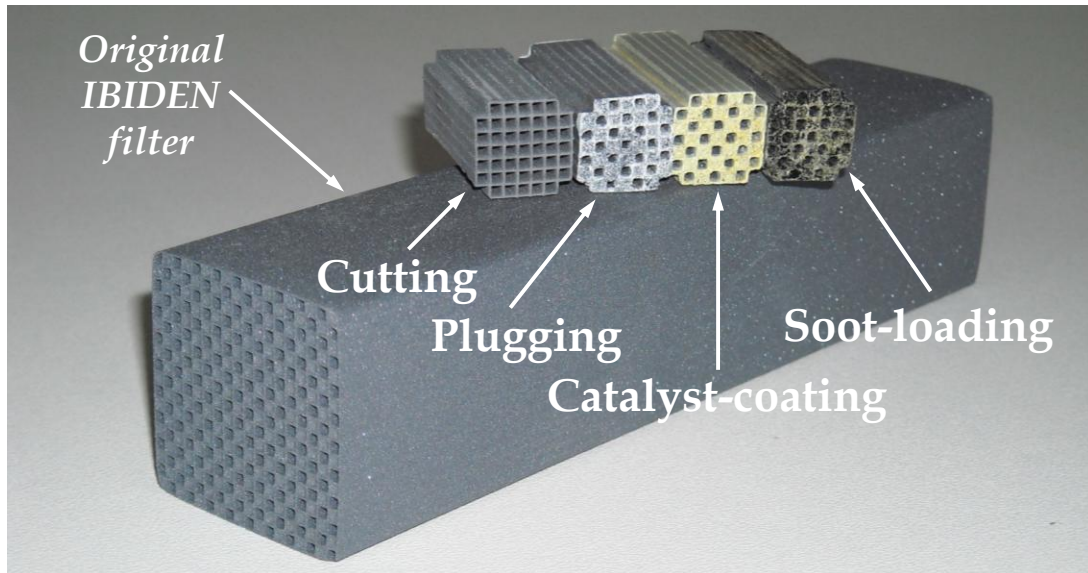


**Figure 7. Monoliths after the stages of cutting, plugging, catalyst-coating and soot-loading (the original IBIDEN filter is also shown).**

## 5.2 Catalytic Filter Characterization

Filter samples (filter as it is, catalyst-coated filter, soot-loaded filter, and filters with two different CeO<sub>2</sub>/soot ratios) were physically characterized.

The pore size distribution (PSD) in the region of macro-pores was evaluated using a Micromeritics Autopore IV by the Hg intrusion porosimetry technique. Specific surface area measurements and micro- and meso-pore analysis were performed with a Quantachrome Autosorb 1-C by N<sub>2</sub> adsorption at 77 K after degassing the samples for 2 h at 150°C. The surface area was evaluated through the BET method, whereas the PSD of micro- and meso-pores was evaluated through the BJH method.

The morphology was observed using a FEI Inspect Scanning Electron Microscope (SEM) equipped with an energy dispersive X-ray (EDX) probe for the elemental mapping.

### 5.3 Apparatus for Regeneration Tests

Figure 8 shows a scheme of the experimental apparatus for the regeneration tests.

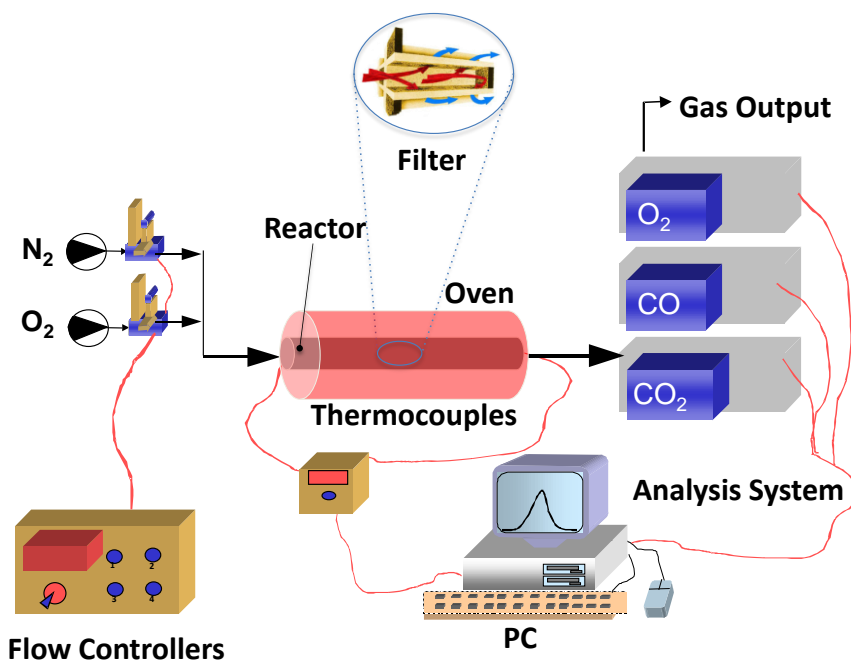


Figure 8. Schematic representation of the experimental apparatus for the regeneration tests.

Figure 9 shows the plant developed at the Laboratory of Catalysis IRC-CNR.



**Figure 9. Plant developed @ the Laboratory of Catalysis IRC-CNR.**

The filter was placed in a tubular quartz reactor (diameter = 2.54 cm). In order to avoid bypass phenomena, the filter was wrapped in a layer of glass wool. The glass wool was previously calcined at 700°C for 5 hours (heating rate of 10°C/min) to eliminate the presence of any organic species. A small piece of foam (with a circular cross-section similar to the cross-section of the filter, and a thickness of about 0.5 cm) was placed upstream the inlet section of the filter to ensure a uniform distribution of the gas flow.

The reactor was placed in a tubular electric oven (LENTON LTD mod. PTF 12/38/500; length = 60 cm; length of the isothermal zone ~ 5 cm) equipped with a PID controller to perform regeneration tests at controlled heating rate. In particular, after preheating up to 250°C in nitrogen stream (at flow rate equal to 0.5 l/h), the system was heated at a rate of 5°C/min up to 700°C.

Brooks 5850S mass flow controllers for N<sub>2</sub> and O<sub>2</sub> were used to set up flow rate and composition of the feed to the reactor. Regeneration tests were performed with total flow rate equal to 47 l/h, and O<sub>2</sub> concentration in N<sub>2</sub> equal to 15 vol. %.

The gas mixture exiting the reactor entered an analysis system including a Fisher-Rosemount NGA2000 analyzer for simultaneous analysis of CO and CO<sub>2</sub> by IR detectors, and O<sub>2</sub> by a paramagnetic detector (no gas sampling probe was used). The filter was weighted before and after each regeneration test to verify the carbon balance through the comparison between the amount of disappeared/consumed soot and the amount of produced CO and CO<sub>2</sub>. The carbon balance was verified with an error of ±10 %.

A by-pass system of the reactor enabled the analysis of the concentration of the gases before entering the reactor, using the same analyzers. Data were continuously recorded on a PC through a data acquisition system developed in LabView environment.

Temperature was measured by two thermocouples suspended in the gas (without touching the wall) and located within the central channel of the filter at about 0.5 cm downstream/upstream of the inlet/outlet section (the foam was appropriately holed to allow their passage). The two thermocouples were type K (Chromel (Ni-Cr) (+)/Alumel (Ni-Al) (-)), with measuring range 200-1260°C and sensitivity of about 41  $\mu\text{V}/^\circ\text{C}$ . They were bare. A blank run ruled out their possible catalytic contribution. Furthermore, owing to the low flow velocities and low temperatures, no convective and radiative thermocouple corrections were required.

An electronic pressure transducer measured the pressure drop across the filter. Finally, the plant was equipped with a safety electro-valve to allow gas to be discharged in the event of accidental excess pressure, and with flow meters to measure the inlet flow rates to the reactor.

Regeneration tests were performed by varying the soot load and, thus, the catalyst/soot ratio from 0 - thermal regeneration - to 98 w/w. In all tests, the two upstream and downstream filter temperatures were substantially the same and followed the expected heating ramp.

All tests were highly repeatable. As an example of such repeatability, Figure 10 shows the concentration of  $\text{CO}_2$  versus temperature as measured during two independent regeneration tests carried out on two filters with catalyst/soot ratio equal to 45 w/w. The two filters were independently prepared following the same procedure (i.e., the four steps of cutting, plugging, catalyst-coating and soot-loading of Figure 7).

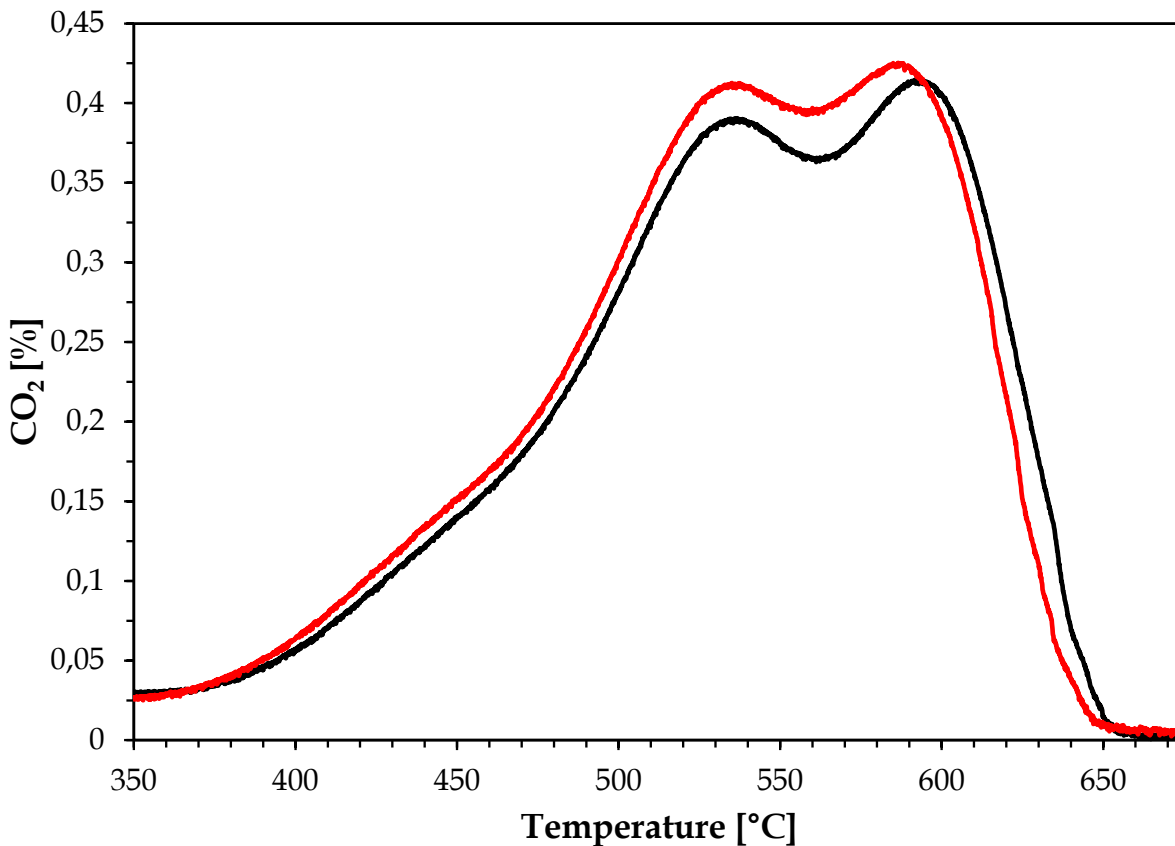


**Figure 10. CO<sub>2</sub> (outlet) concentration (mole percentage) versus temperature as measured during two independent regeneration tests carried out on filters with catalyst/soot ratio equal to 45 w/w.**

In Figure 11, the profiles of CO<sub>2</sub> concentration versus temperature are shown as registered during two catalytic regeneration tests: a first test performed on a “fresh” filter (coated using a colloidal suspension of CeO<sub>2</sub>); a second test performed on an “aged” filter, i.e., the filter regenerated during the first test. For the fresh filter, the catalyst/soot ratio was 35; whereas, for the aged filter, it was 100. The same procedure was used to load both filters with soot. However, after the first regeneration test, it was not possible to get the same soot loading as before.

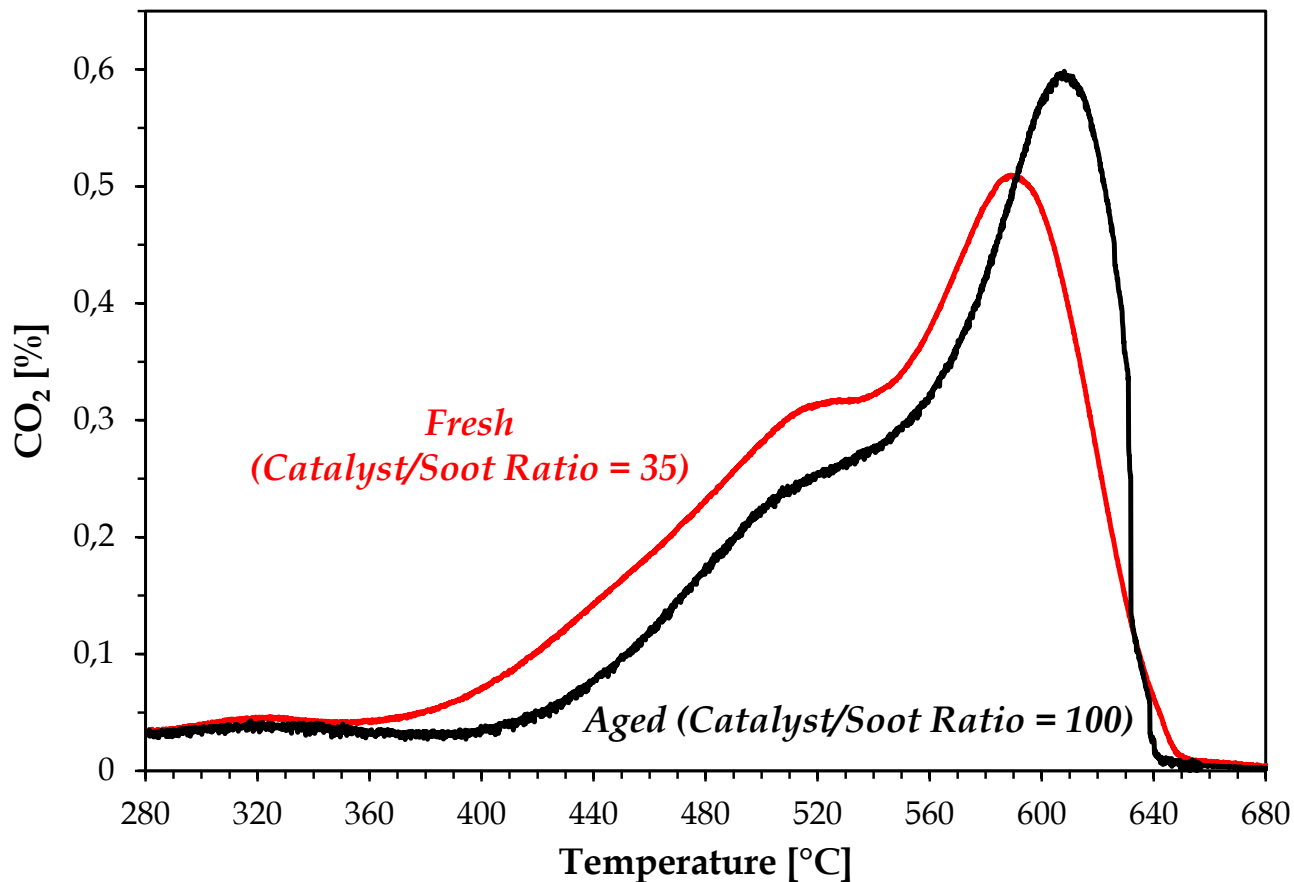


Figure 11. CO<sub>2</sub> concentration versus temperature for “fresh” catalytic filter and “aged” catalytic filter (the filter was coated using a colloidal suspension of CeO<sub>2</sub>).

The figure shows that, in spite of the fact that the aged filter worked with a higher catalyst/soot ratio and, thus, under more favorable conditions of contact between soot and catalyst, a loss in catalytic performance occurred in going from the fresh to the aged filter.

## 6. Results and Discussion

### 6.1. Regeneration Tests

#### 6.1.1 Thermal Regeneration

Figure 12 shows the results obtained from the thermal regeneration test, in terms of CO<sub>2</sub> and CO concentration as a function of the filter temperature.

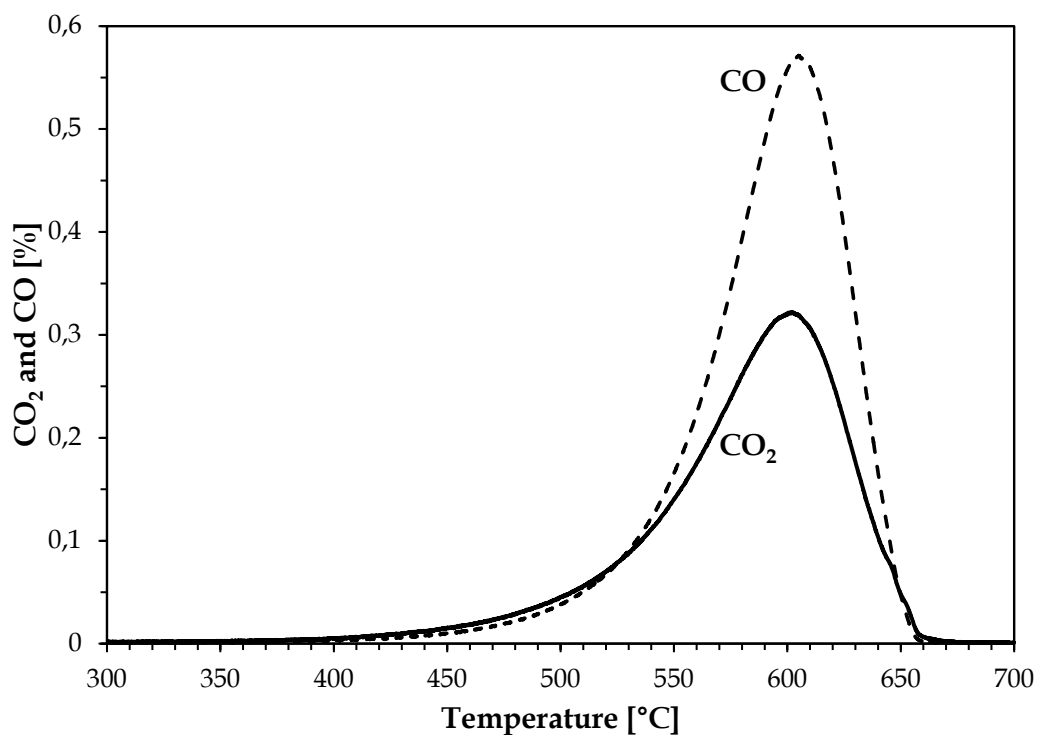


**Figure 12. CO<sub>2</sub> and CO concentration as a function of the filter temperature: Soot-loaded un-catalyzed filter.**

Both profiles exhibit a peak at around 600°C. The ratio between the areas of the two profiles provided a selectivity to CO<sub>2</sub> of about 40 %. Thus, during the thermal regeneration, most of the soot is converted into CO (rather than into CO<sub>2</sub>). Rico Pérez and Bueno-López [2015]

found a similar value of selectivity to CO<sub>2</sub> (51 %) in their tests of thermal regeneration of DPFs.

### 6.1.2 Comparison between Thermal and Catalytic Regeneration

In Figure 13, the results of Figure 12 (thermal regeneration, TR - black curves) are plotted in comparison with the results obtained from a catalytic regeneration test (CR - red curves) performed on a filter having catalyst/soot ratio equal to 20 w/w using ceria obtained starting from a colloidal suspension.

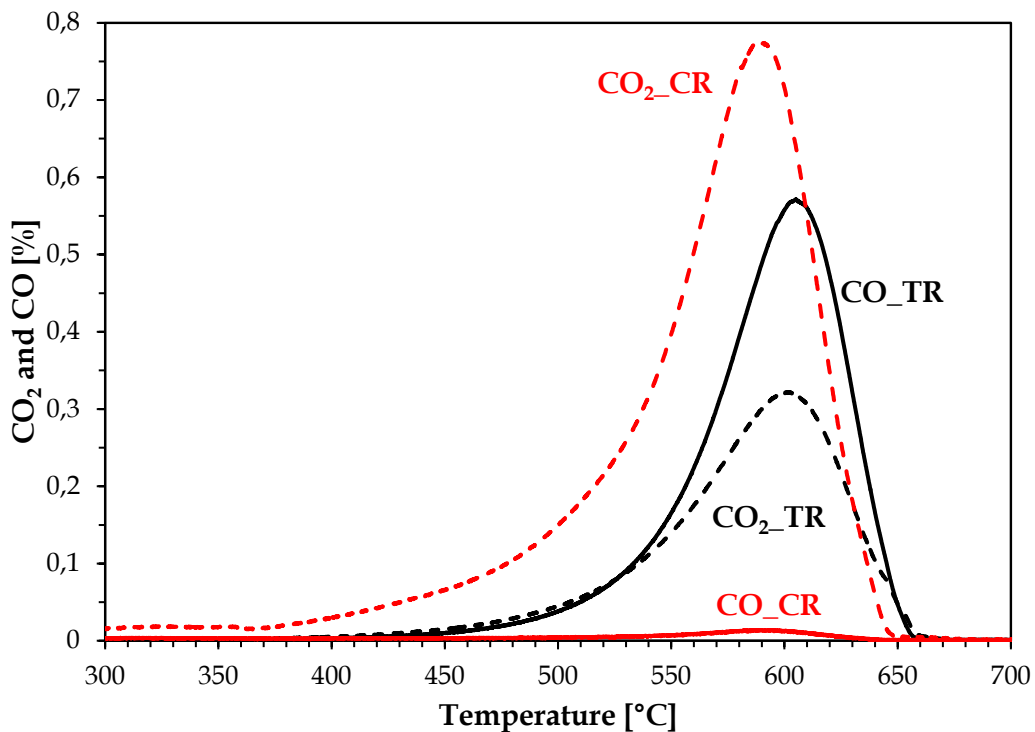
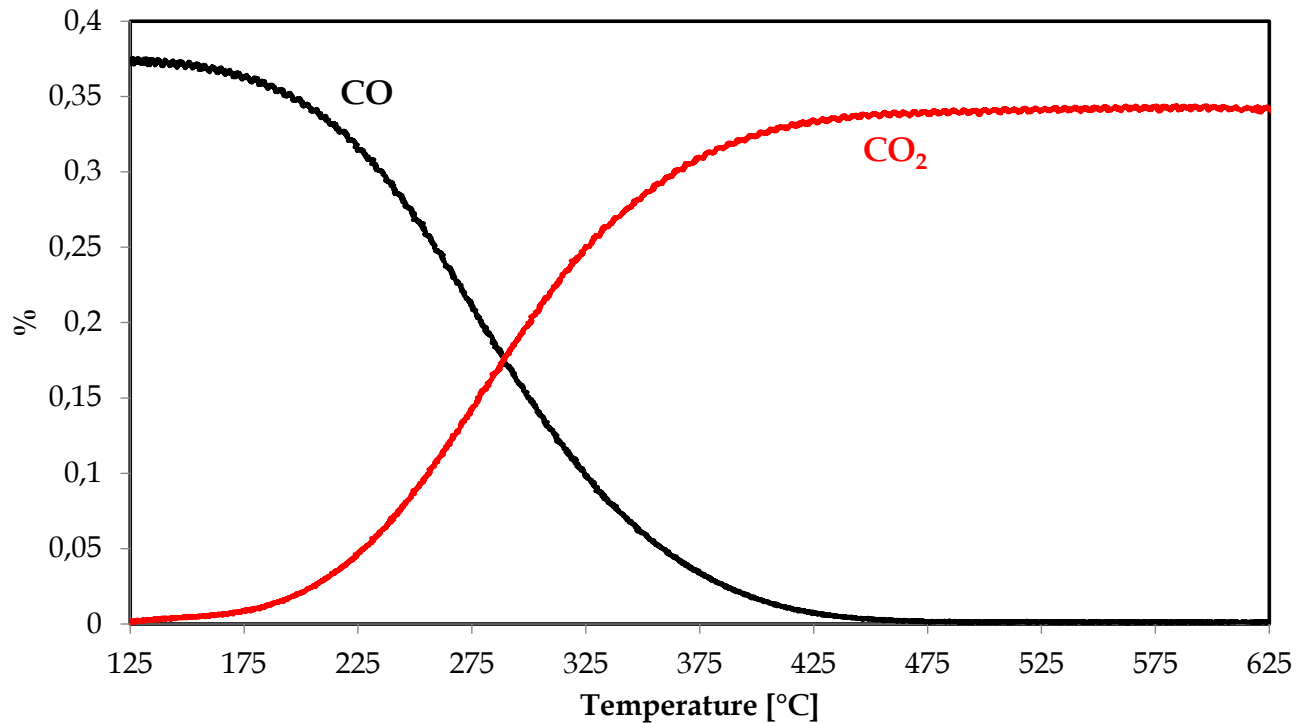


Figure 13. CO<sub>2</sub> (dashed lines) and CO (solid lines) concentration as a function of the filter temperature: Thermal regeneration (black curves) and catalytic regeneration (red curves; catalyst/soot ratio = 20 w/w).

It is worth saying that the results from all the catalytic regeneration tests were scaled using a multiplying factor equal to  $m_{\text{soot\_TR}}/m_{\text{soot\_CR}}$ , where  $m_{\text{soot\_TR}}$  is the mass of soot loaded for the thermal regeneration test (0.048 g), and  $m_{\text{soot\_CR}}$  is the mass of soot loaded for the catalytic regeneration test. The same multiplying factor was used for the results of Figure 10 and Figura 11. Thus, both profiles of CO<sub>2</sub> and CO as well as their underlying areas are directly comparable. When moving from thermal to catalytic regeneration, the concentration profiles shift towards slightly lower temperatures (the shift is of around 10°C). Indeed, the most apparent effect of the catalyst presence is on the selectivity to CO<sub>2</sub>, which increases from ~40 % (TR) to ~98 % (CR). This means that the catalyst activates the CO oxidation. Similar values of selectivity to CO<sub>2</sub> (~95 %) were found during regeneration tests of DPFs loaded with an optimized ceria-praseodymia active phase [Rico Pérez, and Bueno-López, 2015].

The above was confirmed by the results reported in Figure 14 that shows the profiles of CO and CO<sub>2</sub> concentration versus temperature obtained from the regeneration test of the filter coated with the same amount of CeO<sub>2</sub> by colloidal suspension with a feed stream of CO in the absence of soot. It is evident as the catalyst activates the CO oxidation.



**Figure 14. CO<sub>2</sub> (red line) and CO (black line) concentration as a function of the filter temperature obtained from the regeneration test of the filter coated with the same amount of CeO<sub>2</sub> by colloidal suspension with a feed stream of CO in the absence of soot.**

The results of the filter characterization have shown that, at low CeO<sub>2</sub>/soot ratio (28 w/w), in addition to the soot particles penetrated into the catalytic filter wall (internal zone), where a good solid-solid contact is established, a rather thick soot cake (external zone) is formed, which is segregated from the catalyst. Thus, the slight shift of the concentration profiles towards lower temperatures can be attributed to the catalytic conversion of a small fraction of the overall soot (i.e., the soot inside the filter wall), whereas most of the soot (i.e., the cake layer) is still converted via the non-catalytic (thermal) path. In other words, the soot-catalyst contact is too weak and, as found in the experiments by Rico Pérez and Bueno-López [2015],

the process of catalytic regeneration is somewhat hindered. However, in the presence of catalyst, almost all the thermally produced CO is converted to CO<sub>2</sub>, being the catalyzed CO oxidation independent of the soot-catalyst contact.

### 6.1.3 Colloidal Suspension of Ceria versus Solution of Cerium Nitrate

The filters were coated using a colloidal suspension of ceria or a solution of cerium nitrate. Figure 15 shows the results obtained from the thermal regeneration (black curves) with those obtained from the regeneration test of the filter coated with CeO<sub>2</sub> by a colloidal suspension (red curves) along with the results obtained from the regeneration test of the filter coated with CeO<sub>2</sub> using the solution of cerium nitrate (blue curves).

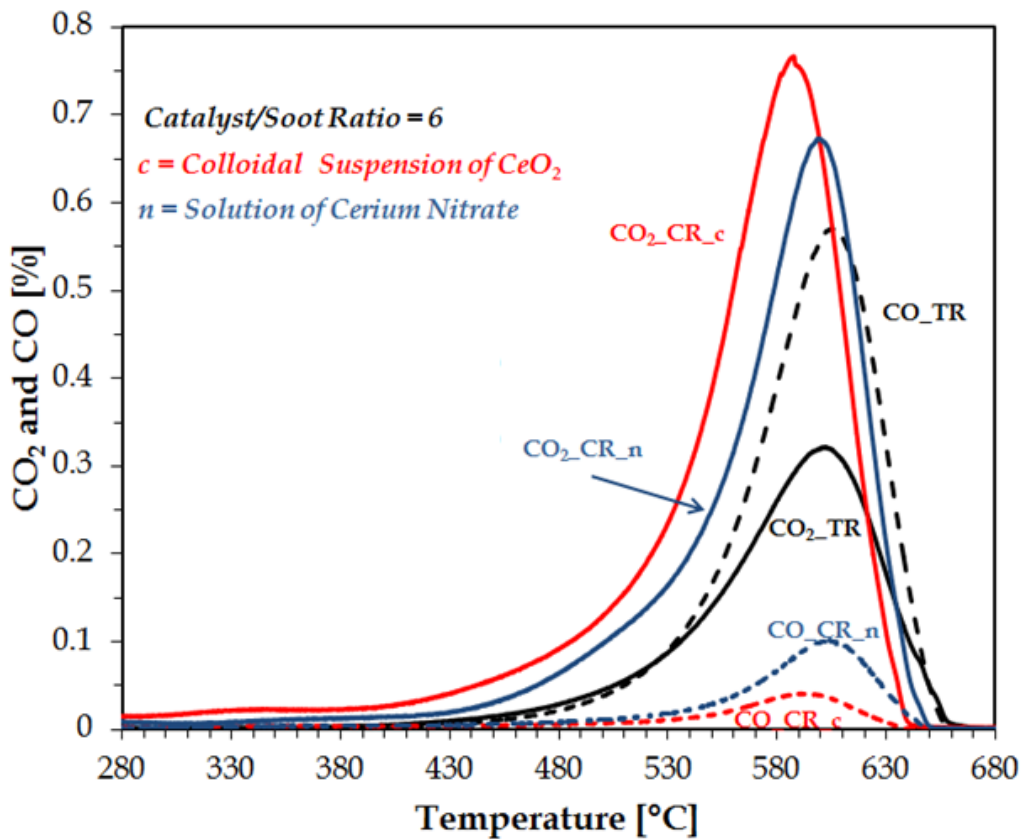
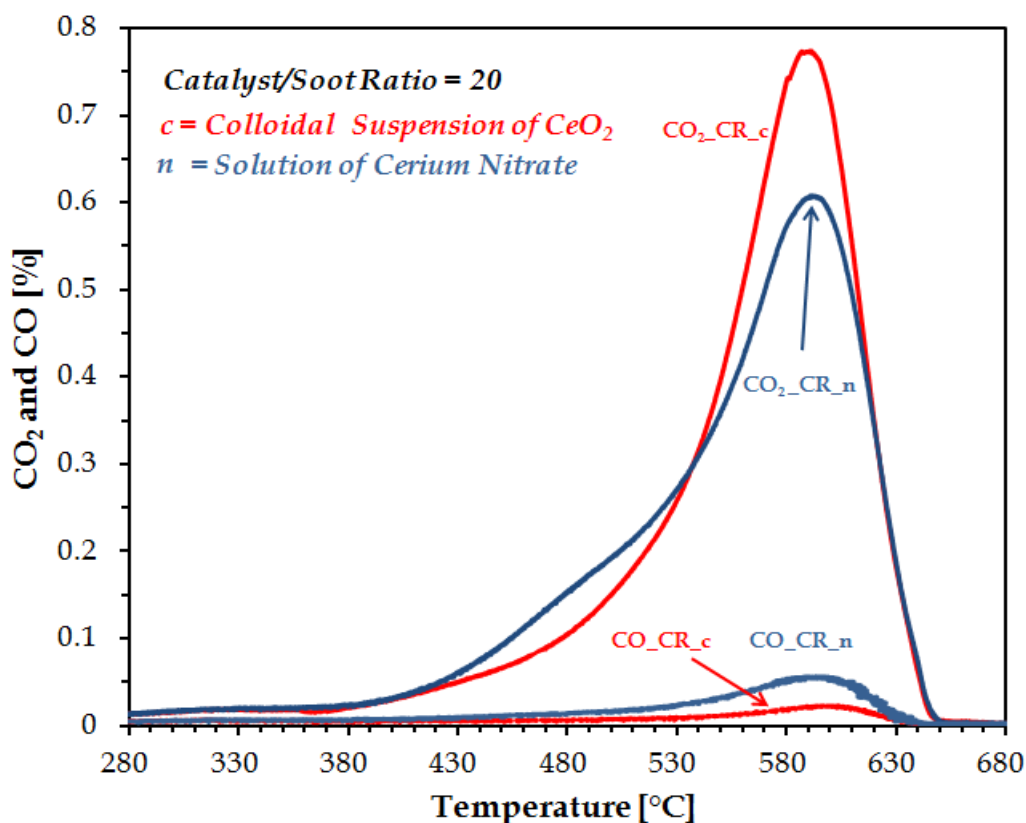


Figure 15. CO<sub>2</sub> and CO concentration versus temperature: Thermal regeneration (black curves) and catalytic regeneration of filters coated using a colloidal suspension of CeO<sub>2</sub> (red curves) and a solution of cerium nitrate (blue curves). For both filters, the catalyst/soot ratio [w/w] was equal to 6.

The figure shows that the filter coated using a colloidal suspension of CeO<sub>2</sub> performs better than the filter coated using a solution of cerium nitrate. In particular, the selectivity to CO<sub>2</sub> is ~95% for the former and ~86% for the latter.

The results of Figure 15 were obtained for catalyst/soot ratio equal to 6. Figure 16 shows the same results for catalyst/soot ratio equal to 20.



**Figure 16. CO<sub>2</sub> and CO concentration versus temperature: Catalytic regeneration of filters coated using a colloidal suspension of CeO<sub>2</sub> and a solution of cerium nitrate. For both filters, the catalyst/soot ratio [w/w] was equal to 20.**

Even for catalyst/soot ratio equal to 20, the filter coated using a colloidal suspension of CeO<sub>2</sub> performs better - in terms of selectivity to CO<sub>2</sub> - than the filter coated using a solution of

cerium nitrate. However, the differences in filter performance decrease with increasing catalyst/soot ratio. In particular, for the filter coated using a colloidal suspension of CeO<sub>2</sub>, the selectivity to CO<sub>2</sub> is equal to ~98%; for the filter coated using a solution of cerium nitrate, it is equal to ~92%.

With the solution of cerium nitrate, the macro-pores of the filter remain substantially free, thus suggesting that a better soot-catalyst contact is established. Nevertheless, in the light of the results of Figures 15 and 16, it can be argued that CeO<sub>2</sub> from the solution of nitrate probably crystallizes in a less active form (or is mainly amorphous) compared to CeO<sub>2</sub> from the colloidal suspension. Indeed, it is widely accepted that cubic ceria is more active towards soot oxidation [see, e.g., Piumetti et al., 2015].

#### **6.1.4 Effect of the Catalyst Morphology**

Figure 17 shows the profiles of CO<sub>2</sub> concentration versus temperature as obtained from regeneration tests of the filters prepared at POLITO and coated with CeO<sub>2</sub> in nanocube shape (black curve) and star shape (blue curve). The figure also shows the CO<sub>2</sub> concentration-temperature profile obtained from the regeneration test of the filter coated with CeO<sub>2</sub> using a colloidal suspension (red curve) (catalyst/soot ratio=98).

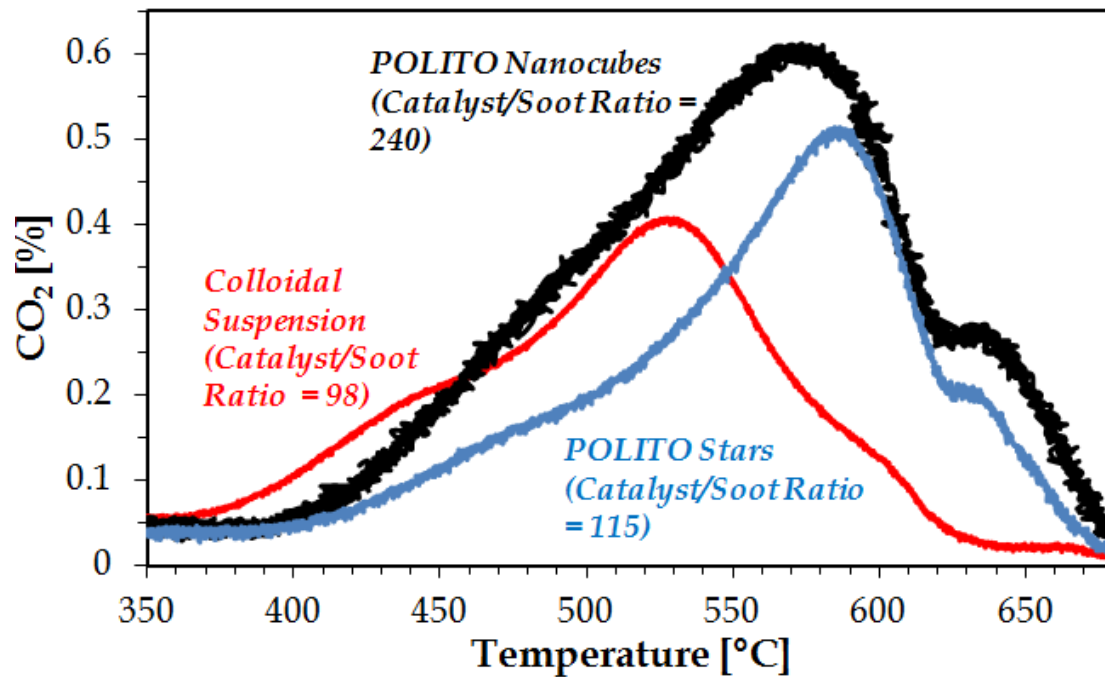
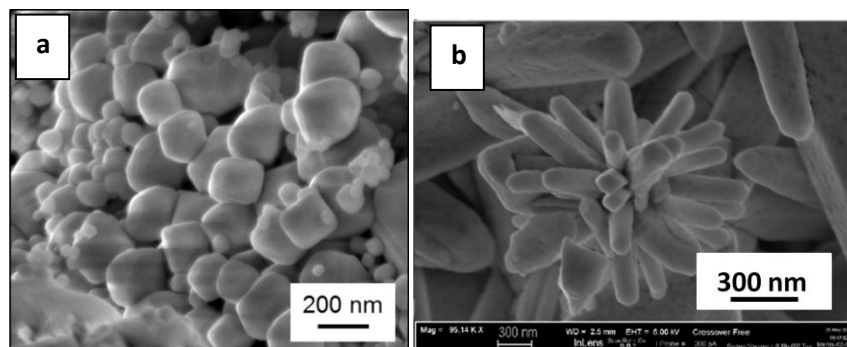


Figure 17. CO<sub>2</sub> concentration versus temperature: Filters coated with CeO<sub>2</sub> in nanocube and star shape (POLITO) and filter coated using a colloidal suspension of CeO<sub>2</sub>.

The selectivity to CO<sub>2</sub> for filter coated using a colloidal suspension of CeO<sub>2</sub> overcomes 99 %, for filters coated with CeO<sub>2</sub> in nanocube shape is equal to ~87% while for the filter coated with CeO<sub>2</sub> in star shape is equal to ~92%. However, quantitative comparison is not possible, being the catalyst/soot ratio of the three filters different (it was difficult to load the POLITO filters with soot). Although the POLITO filters work with a higher catalyst/soot ratio and, thus, under more favorable conditions of contact between soot and catalyst than those of the filter coated with colloidal ceria, they show the worst performance in terms both of selectivity to CO<sub>2</sub> and the highest temperature values corresponding to peaks of CO<sub>2</sub> profiles.

Figure 18 [from Piumetti et al., 2015] shows SEM images of CeO<sub>2</sub> in nanocube (a) and star shape (b). CeO<sub>2</sub> obtained by a colloidal suspension of CeO<sub>2</sub> nanoparticles (10-20 nm) performs better than CeO<sub>2</sub> in nanocube shape, and CeO<sub>2</sub> in star shape. This goal is reached thanks to the lower size (10-20 nm) of CeO<sub>2</sub> obtained by a colloidal suspension than that of CeO<sub>2</sub> in nanocube shape (200 nm), and CeO<sub>2</sub> in star shape (300 nm). For this reason both CeO<sub>2</sub> in nanocube shape and in star shape are not able to establish a good contact with the soot which results in the worst performance.



**Figure 18. SEM images of CeO<sub>2</sub> in nanocube (a) and star shape (b) from Piumetti et al., 2015.**

## 6.2. Chemical and Physical characterization

### 6.2.1 Filter Characterization

Macro-pores of the original filter, evaluated by Hg porosimetry, account for 46 % porosity, in good agreement with the value provided by the supplier (42 %).

Figure 19 shows the pore size distribution (PSD) in the region of macro-pores for four samples: original filter, CeO<sub>2</sub>-coated filter and two filters with different CeO<sub>2</sub>/soot ratios.

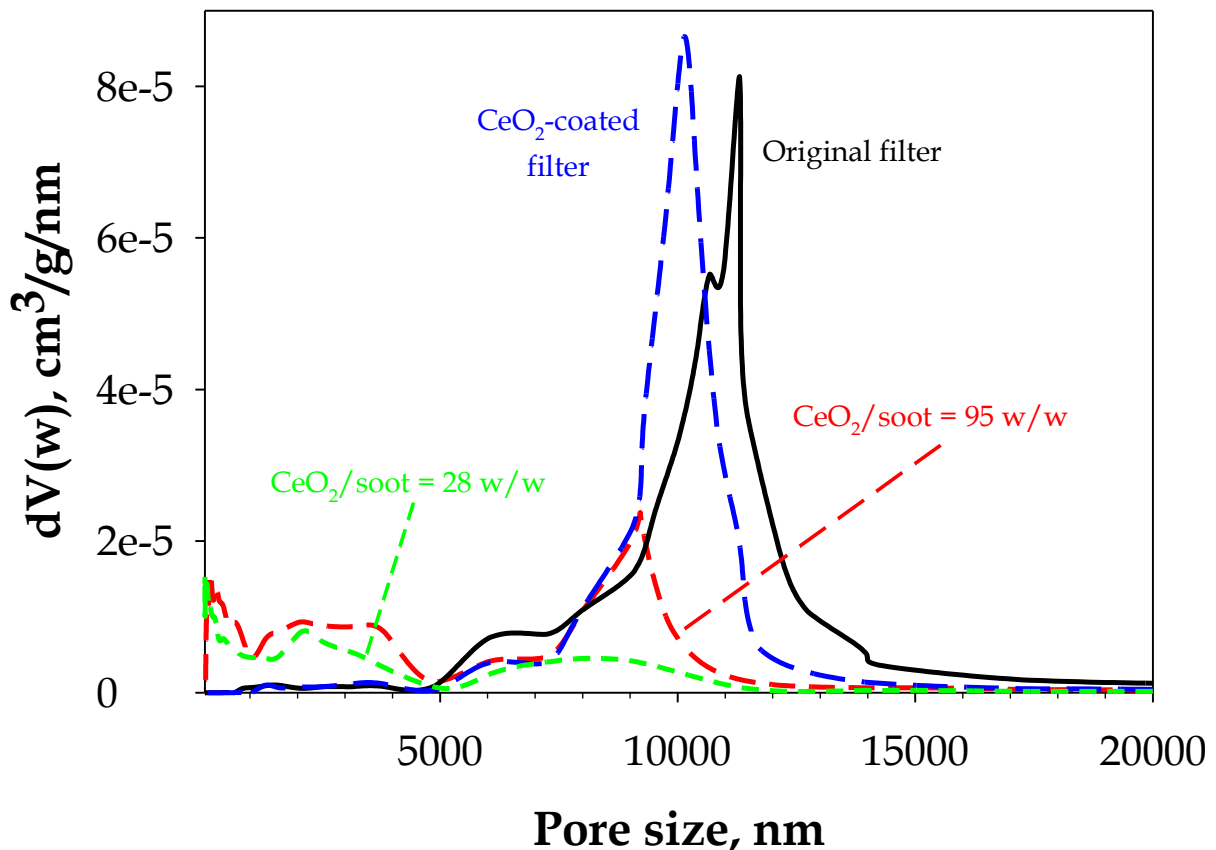
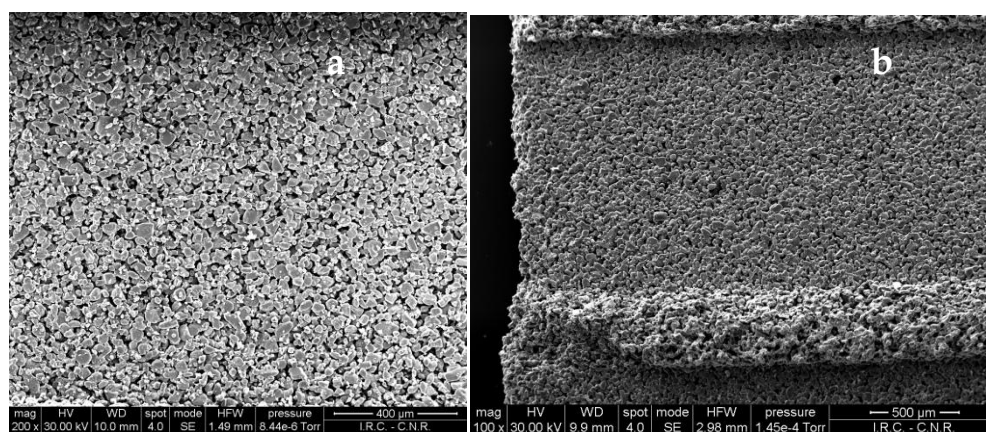


Figure 19. Pore size distribution (PSD) in the region of macro-pores for original filter, CeO<sub>2</sub>-coated filter and two filters with different CeO<sub>2</sub>/soot ratios.

The original filter exhibits a quite narrow pore distribution peaked at 11000-12000 nm, resulting from SiC inter-particle spaces. After the catalyst-coating, the pore distribution slightly changes, showing a peak at about 10000 nm. This suggests that the deposition of ceria nanoparticles inside the filter walls results in a limited occlusion of macro-pores, thus preserving the filtering properties. On the contrary, the soot loading results in a progressive reduction of the fraction of large macro-pores, along with the appearance of smaller pores (< 5000 nm). This means that an occlusion of large macro-pores occurs.

The SEM images of Figure 20 show the channel surface of the original filter (a) and that of the CeO<sub>2</sub>-coated filter (b).



**Figure 20. SEM images of the channel surface: Original filter (a); CeO<sub>2</sub>-coated filter (b).**

The typical granular structure of the SiC filter (i.e., the network of SiC particles) is still preserved after the catalyst deposition, thus confirming the results obtained by Hg porosimetry. The ceria nanoparticles penetrate into the macro-pores avoiding the accumulation of a catalyst layer on top of the filter wall.

In Table 4, the specific surface area and the pore volume (i.e., the volume of micro- and meso-pores) are reported for the original filter, the soot-loaded filter, the CeO<sub>2</sub>-coated filter and the two filters with different CeO<sub>2</sub>/soot ratios.

**Table 4. Specific surface area and pore volume (i.e., volume of micro- and meso-pores) for original filter, soot-loaded filter, CeO<sub>2</sub>-coated filter, and two filters with different CeO<sub>2</sub>/soot ratios.**

<b>Sample</b>	<b>Specific surface area (m<sup>2</sup>/g)</b>	<b>Pore volume (cm<sup>3</sup>/g)</b>
Original filter	3	0.0033
Soot-loaded filter	10	0.017
CeO <sub>2</sub> -coated filter	16	0.022
Filter with CeO <sub>2</sub> /soot ratio = 95 w/w	22	0.033
Filter with CeO <sub>2</sub> /soot ratio = 28 w/w	24	0.034

The specific surface area of the original filter is very low as well as the pore volume. The deposition of CeO<sub>2</sub> and soot leads to an increase of both surface area and pore volume. This can be linked to the decrease of macro-pore size and (especially in the case of soot deposition) volume, which is counterbalanced by the increase of micro- and meso-pores, and also to the contribution of micro- and meso-pores intrinsically present in both ceria and soot. In going from the original filter to the filter with CeO<sub>2</sub>/soot ratio equal to 28 w/w, the overall amount of ceria + soot increases and, thus, micro- and meso-pores increase as well. However, the combined effect of ceria and soot is less than additive.

The PSD in the region of micro- and meso-pores shown in Figure 21 confirms the above considerations.

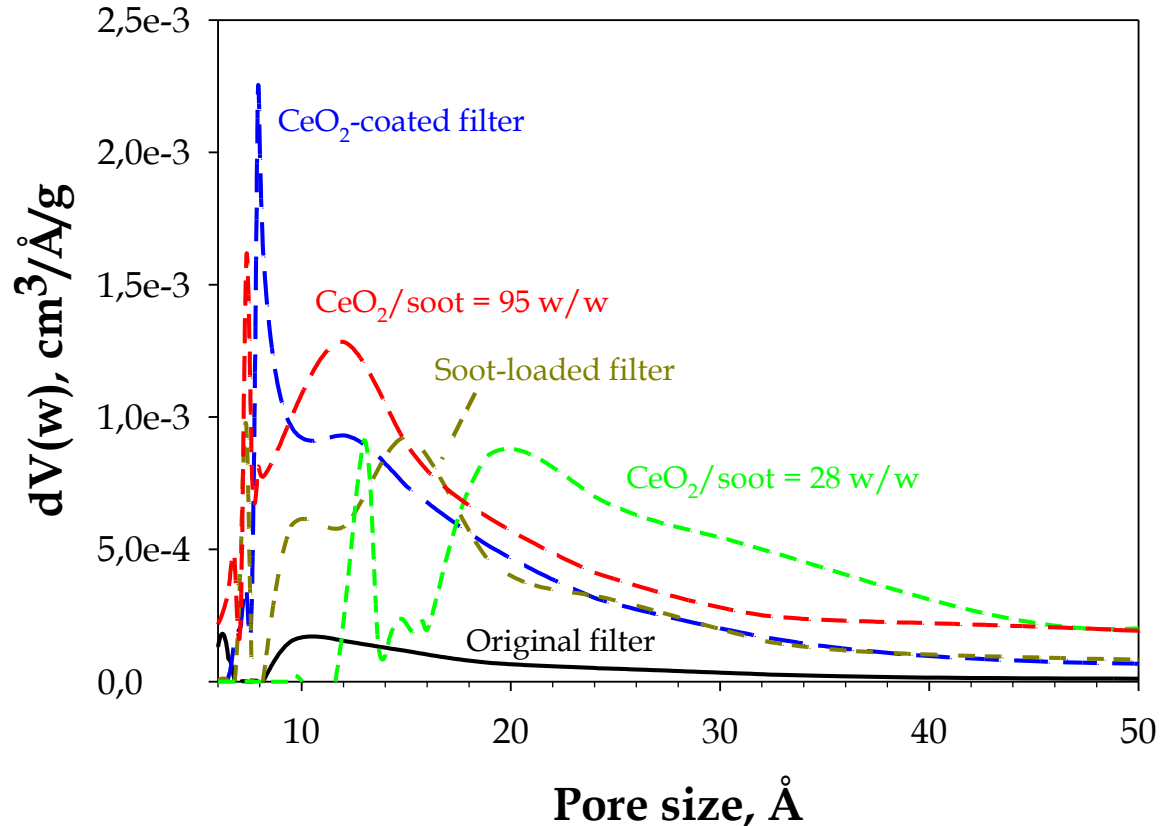


**Figure 21. Pore size distribution (PSD) in the region of micro- and meso-pores for original filter, soot-loaded filter, CeO<sub>2</sub>-coated filter, and two filters with different CeO<sub>2</sub>/soot ratios.**

The CeO<sub>2</sub> coating results in a large increase of pores in the range 10-40 Å, along with a more pronounced micro-porosity peaked at around 7 Å. The soot-loaded filter exhibits pores in the same range as the catalyst-coated filter, even if more centered at higher size.

The surface area and the pore volume both increase when ceria and soot are simultaneously present on the filter providing very similar values (Table 4). Nevertheless, the PSD is different depending on the CeO<sub>2</sub>/soot ratio. At high CeO<sub>2</sub>/soot ratio (95 w/w), the average pore size is centered at lower values, whilst at low CeO<sub>2</sub>/soot ratio (28 w/w), there is a larger contribution of pores with size higher than 20 Å.

It is worth highlighting that the data related to the changes in exposed surface area and porosity, when the filter is first coated with catalytic material and then loaded with soot, are likely to be very useful in modelling the operation of this technology.

### **6.3. Effect of the Catalyst/Soot Ratio**

As previously described CeO<sub>2</sub> obtained by a colloidal suspension shows a better activity than CeO<sub>2</sub> obtained by a solution of cerium nitrate, on the other hand the deposition of ceria nanoparticles (obtained by a colloidal suspension) inside the filter walls results in a limited occlusion of macro-pores, thus preserving the filtering properties. Therefore the contact between the catalyst (CeO<sub>2</sub> obtained by a colloidal suspension) and the soot has been investigated.

### 6.3.1 Effect of the Catalyst/Soot Ratio “with cake”

Figure 22 shows the plots of normalized  $\text{CO}_x$  ( $= \text{CO}_2 + \text{CO}$ ) concentration versus temperature for catalyst/soot ratio varying from 0 (thermal regeneration) to 65 w/w. For the catalytic tests,  $\text{CO}_x$  is substantially  $\text{CO}_2$  - this especially true for catalyst/soot ratio  $\geq 35$  w/w, when the selectivity to  $\text{CO}_2$  overcomes 99 %.

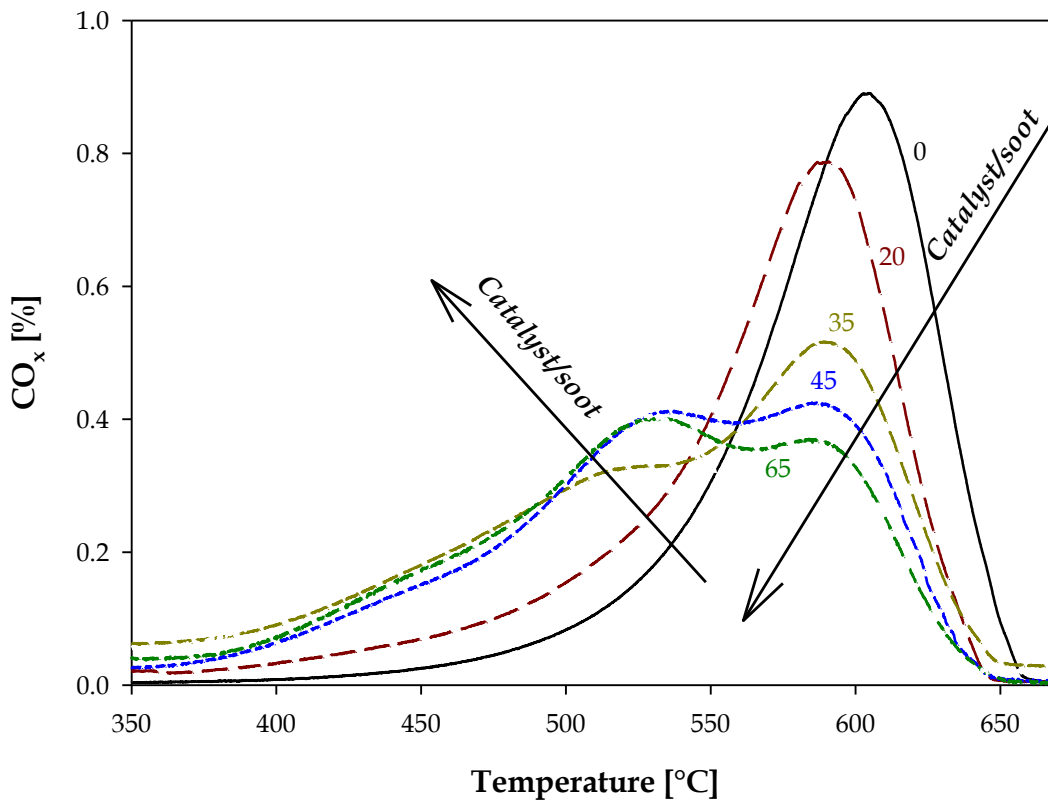


**Figure 22.  $\text{CO}_x$  ( $= \text{CO}_2 + \text{CO}$ ) concentration as a function of the filter temperature for different catalyst/soot ratios (w/w).**

Starting from catalyst/soot ratio equal to 35 w/w, a double-peaked shape appears. The higher temperature peak is still centered at  $\sim 590^\circ\text{C}$  (as the peak observed at catalyst/soot

ratio equal to 20 w/w), whereas the lower temperature peak is centered at  $\sim 520^{\circ}\text{C}$  and exhibits a shoulder at  $\sim 450^{\circ}\text{C}$ . In these conditions the regeneration is essentially thermal. On the other hand, the results of the filter characterization have shown that, at these catalyst/soot ratios, a soot cake layer accumulates on top of the catalytic walls of the filter, thus resulting in a large fraction of soot burned via thermal path, due to the poor cake-catalyst contact, and thus, in much worse regeneration performance. However, in the presence of catalyst, almost all the thermally produced CO is converted to  $\text{CO}_2$ , being the catalyzed CO oxidation independent of the soot-catalyst contact. The limited contact between the soot particles and the catalyst affects the catalytic action even in terms of the dynamics of regeneration. In fact high temperature front motion may lead to excessive temperature rise [Martirosyan et al., 2010]. The moving front temperature and velocity increase with increasing oxygen concentration and soot load [Chen et al., 2009a] while the maximum soot layer temperature occurs at the gas-soot interface [Chen et al., 2011a]. Therefore, it was conjectured that the temperature excursion that melts the DPF is a dynamic response to a sudden change in the engine load. In particular, the filter melting was attributed to a transient temperature excursion caused by a rapid shift of a car from normal driving to idle during regeneration [Chen et al., 2009b; 2010; 2011b].

### 6.3.2 Effect of the Catalyst/Soot Ratio “without cake”

Figure 23 shows the plots of normalized  $\text{CO}_x$  ( $= \text{CO}_2 + \text{CO}$ ) concentration versus temperature for catalyst/soot ratio equal to 98 w/w (red curve) along with those of Figure 22 for catalyst/soot ratios equal to 0 (black curve) and 20 (brown curve).

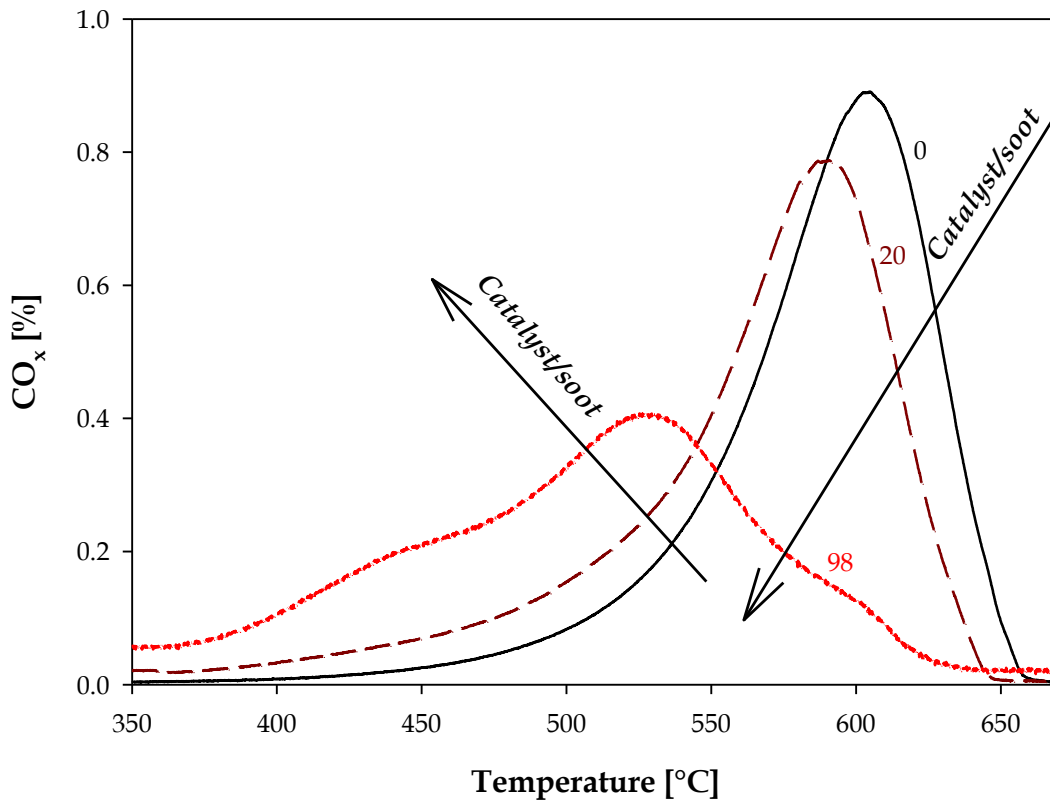


**Figure 23.**  $\text{CO}_x$  ( $= \text{CO}_2 + \text{CO}$ ) concentration as a function of the filter temperature for catalyst/soot ratios (w/w) equal to 0 (black curve), 20 (brown curve), 98 (red curve).

The lower temperature contribution becomes almost the unique one for catalyst/soot ratio equal to 98 w/w. On the other hand, the results of the filter characterization have shown that, at high  $\text{CeO}_2$ /soot ratio (95 w/w), a very thin cake layer is formed and most of the soot particles deeply penetrate into the macro-pores of the filter wall, where the catalyst is highly

dispersed, thus resulting in a very effective solid-solid contact. Thus, the lower temperature peak can be reasonably attributed to the catalyzed conversion of soot.

### 6.3.3 "Cake" versus "No cake"

Figure 24 shows  $\text{CO}_x$  ( $= \text{CO}_2 + \text{CO}$ ) concentration as a function of the filter temperature for catalyst/soot ratios (w/w) equal to 0 (black curve), 20 (blue curve), 98 (red curve).

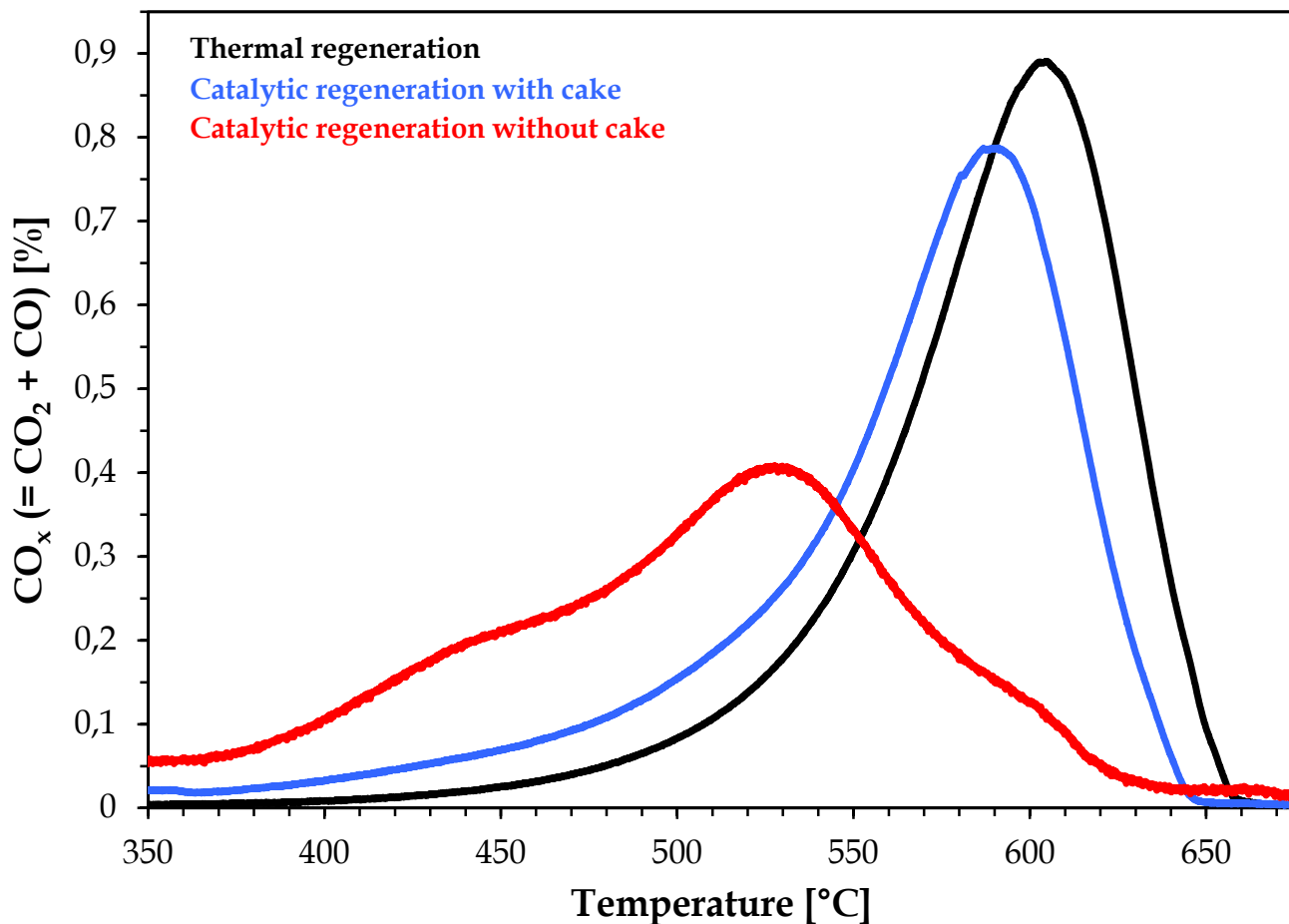
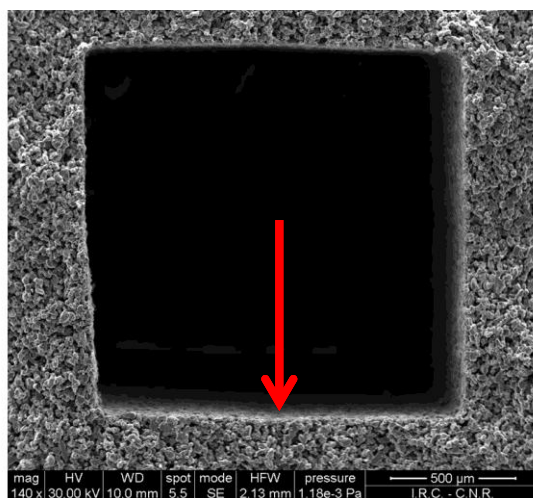


Figure 24.  $\text{CO}_x$  ( $= \text{CO}_2 + \text{CO}$ ) concentration as a function of the filter temperature for catalyst/soot ratios (w/w) equal to 0 (black curve), 20 (blue curve), 98 (red curve).

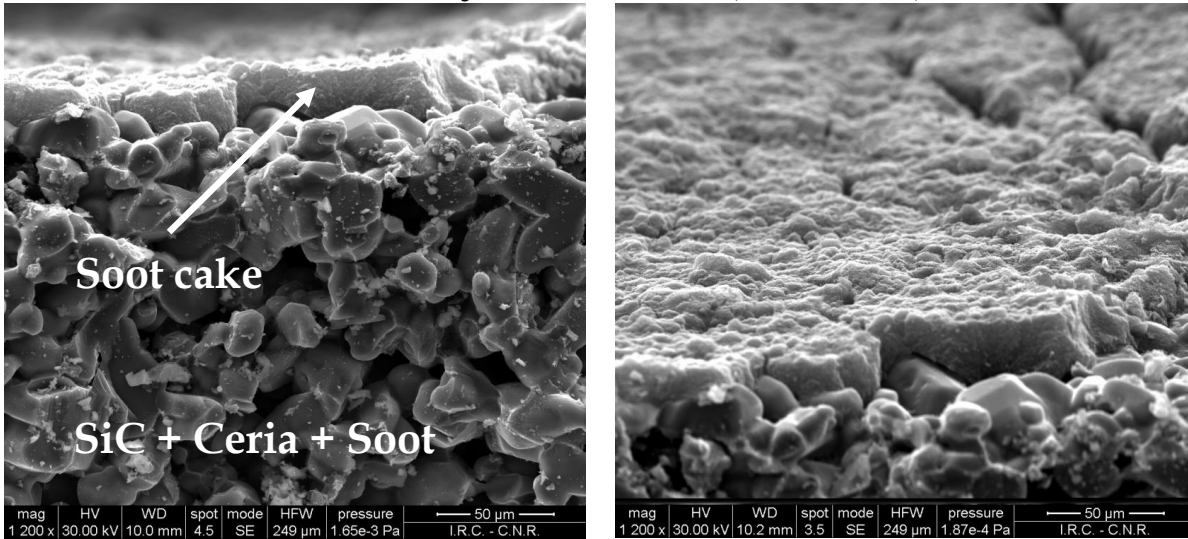
The better regeneration performance is found with increasing catalyst/soot ratio. This is a direct consequence of the decreased cake thickness and, thus, of the decreased role played by the external zone with respect to that played by the internal one (catalytic filter wall). Indeed, as the cake thickness is decreased, overall better conditions of soot-catalyst contact are established, which allow to move from a catalyst-assisted thermal regeneration mode (catalyst/soot ratio = 20; 35; 45; 65 w/w) to an almost purely catalytic regeneration mode (catalyst/soot ratio = 98 w/w). In the case of the catalyst-assisted thermal regeneration mode, a double-step oxidation mechanism takes place: 1) internal zone - catalytic soot oxidation to CO<sub>2</sub>; 2) external zone - thermal oxidation of the soot cake mainly to CO, which is catalytically oxidized to CO<sub>2</sub> at higher temperature. In the case of the almost purely catalytic regeneration mode, the cake layer is almost undetectable and soot oxidation substantially occurs according to step 1) (step 2) plays a minor role).

Figure 25 shows the SEM images of the cross section of the filter channel. Figure 26 is obtained by Figure 25 zooming in the area where the arrow is pointing.



**Figure 25. SEM images of the cross section of the filter channel.**

**Low catalyst/soot ratio (= 28 w/w)**



**High catalyst/soot ratio (= 95 w/w)**

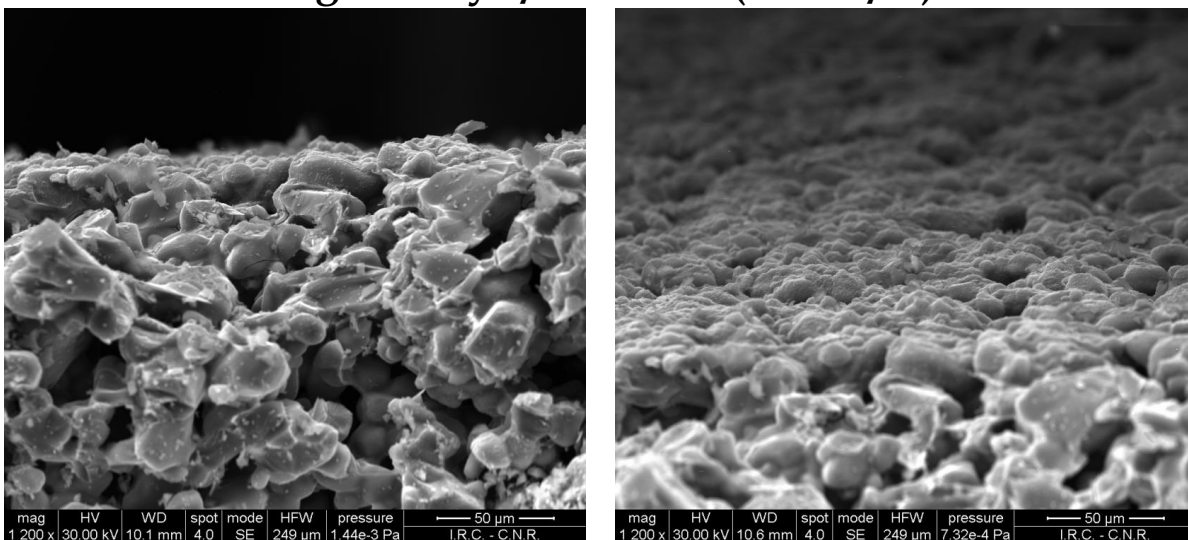


**Figure 26. SEM images of cross section of filter channel for two samples with low (top) and high (bottom)  $\text{CeO}_2$ /soot ratio. In the left pictures, the samples are perpendicular to the radiation; in the right pictures, the tilt angle of radiation is higher than 90 degrees.**

In Figure 26, the SEM images of the cross section of the filter channel are shown for the two samples with low (top) and high (bottom)  $\text{CeO}_2$ /soot ratio. In the left pictures, the samples

are perpendicular to the radiation; in the right pictures, the tilt angle of radiation is higher than 90 degrees to better show the morphology of the soot deposition onto the channel surface. These images, along with the results of the EDX elemental mapping shown in Figure 27, are useful to describe the interaction occurring among soot, catalyst and SiC.

At low  $\text{CeO}_2$ /soot ratio (28 w/w), i.e., in the presence of high amount of soot, the typical soot cake (thickness of around 15-20  $\mu\text{m}$ ) appears on the surface of the filter wall, in addition to a small fraction of soot that deeply penetrates into the filter macro-pores coming in close touch with highly dispersed ceria. This is also confirmed by the EDX elemental distribution of Figure 27 (top).

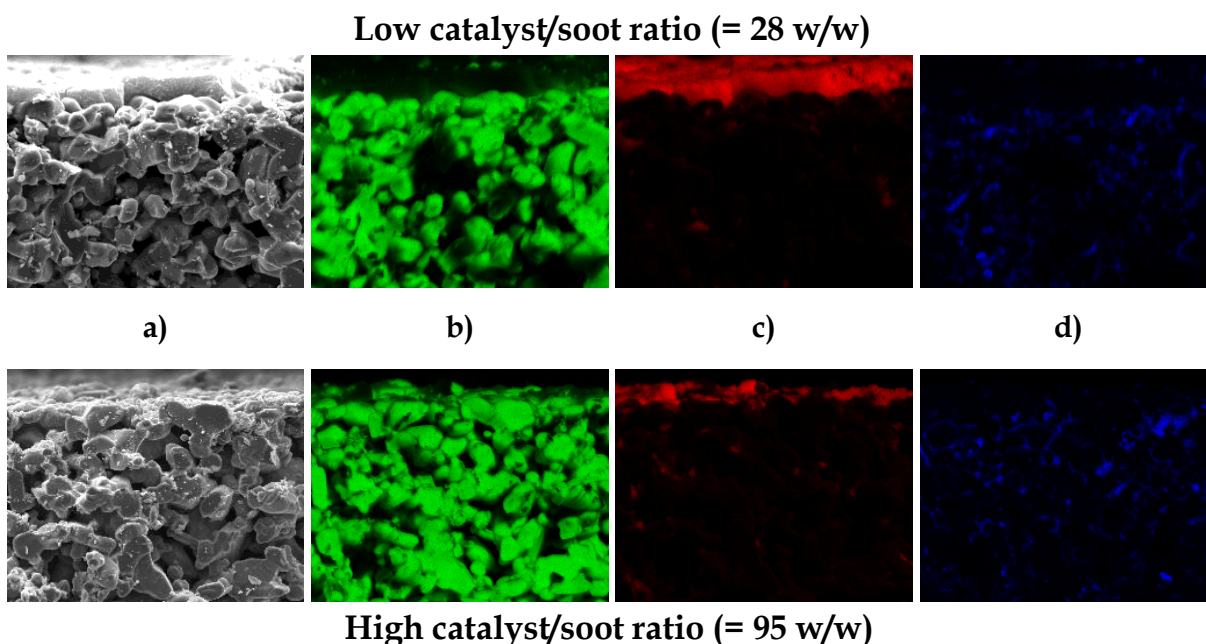


**Figure 27. EDX mapping of cross section of filter channel for two samples with low (top) and high (bottom)  $\text{CeO}_2$ /soot ratio: (a) SEM images and distribution of (b) Si, (c) C, (d) Ce.**

Yapaulo et al. [2009] found the same kind of soot distribution in a real DPF: some soot deeply penetrates into the wall, whereas the majority of soot stays very close to the wall surface.

It is worth noting that the soot-ceria contact conditions established inside the filter wall look like those reported by Bensaïd et al. [2013] in the case of the fibrous ceria morphology, i.e., a network of fibers which surround the soot particles, thus maximizing the number of contact points. On the other hand, the size of the ceria aggregates inside the filter wall is below 20  $\mu\text{m}$  and that of the penetrated soot particles even smaller, condition that can virtually promote a good soot-catalyst contact. Indeed, Iojoiu et al. [Iojoiu et al., 2008] reported that, when applying “highly tight” contact conditions to powder samples (i.e., when ball milling ceria and soot), the soot-catalyst aggregates show a bi-modal distribution of the particle sizes with the main peak centered at about 15  $\mu\text{m}$ .

At high  $\text{CeO}_2$ /soot ratio (95 w/w), the cake layer becomes very thin, although the morphology of the soot deposition onto the channel surface seems to be very similar to that of the other sample. The EDX results of Figure 27 (bottom) confirm the very small cake thickness, along with the incorporation of  $\text{CeO}_2$  and soot inside the filter macro-pores. Thus, the high  $\text{CeO}_2$ /soot ratio assures a better soot-catalyst contact, avoiding a large accumulation of soot onto the filter wall in the form of cake layer, which is substantially segregated from the catalyst.

Figures 26 and 27 allow a clear distinction between two filter zones: an internal zone, which is the catalytic porous wall of the filter, and an external zone, which is the cake layer. At low  $\text{CeO}_2$ /soot ratio, the external zone is well distinct from the internal one, whereas at high  $\text{CeO}_2$ /soot ratio, it is quite negligible, the soot particles being almost totally included inside

the filter macro-pores. Therefore the results have demonstrated that there exist conditions of contact between soot and ceria and, more precisely, conditions of distribution of soot inside and on top of the catalytic porous wall of the filter, that allow a catalytic - rather than thermal - regeneration mode to be established. Under such conditions, soot oxidation may occur at low temperatures, thus avoiding sintering and deactivation of ceria. This means that strategies able to maximize the soot-ceria contact will limit the temperature necessary for regeneration, thus preserving the catalyst itself. In order to quantify the role played by both external and internal zones in affecting the regeneration performance, temperature programmed combustion tests were performed on filters with catalyst/soot ratio varying from 0 (thermal regeneration) to 98 w/w.

In order to quantitatively assess the fraction of catalytically converted soot (with respect to the overall amount of combusted soot), the deconvolution of the  $\text{CO}_x$  concentration curves into the two (catalytic and thermal) contributions was performed. To this end, the Fityk software (free version 0.9.1) was used [Wojdyr, 2010].

Figure 28 shows the fraction of catalytically converted soot (along with the complementary fraction of thermally converted soot) as a function of the catalyst/soot ratio.

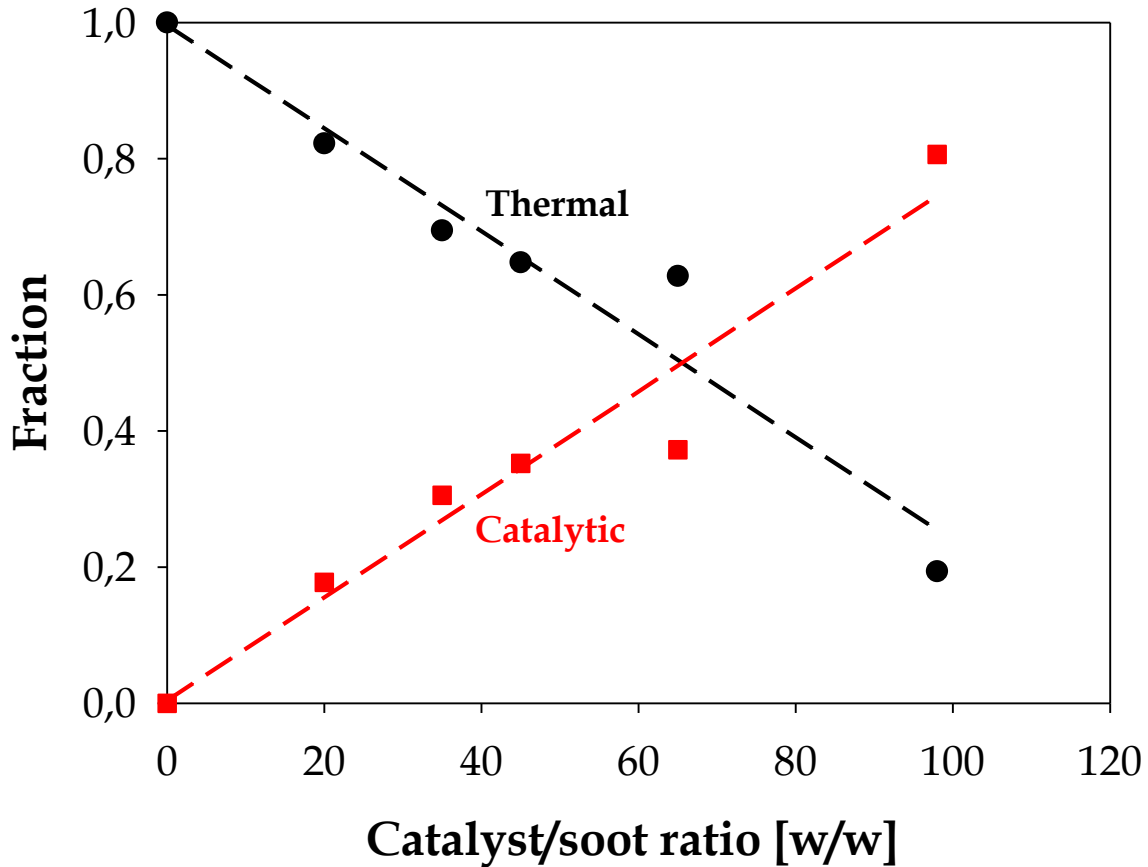
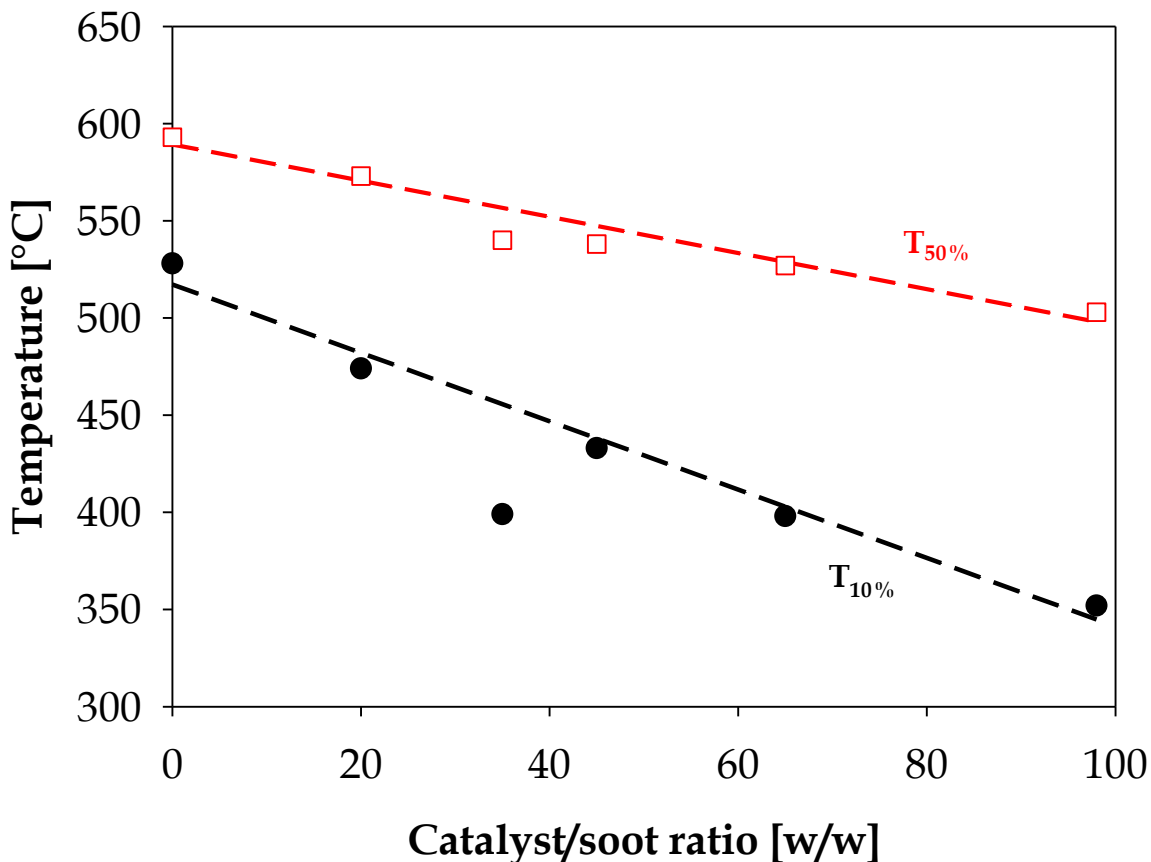


Figure 28. Fraction of catalytically converted soot (along with the complementary fraction of thermally converted soot) as a function of the catalyst/soot ratio.

The fraction of catalytically converted soot increases roughly linearly with increasing catalyst/soot ratio. In particular, for the ratios corresponding to the catalyst-assisted thermal regeneration mode (20; 35; 45; 65 w/w), the catalytic fraction is always lower than 0.5. Conversely, for the almost purely catalytic regeneration mode (98 w/w), it is equal to around 0.8.

To quantify the improvement in terms of regeneration performance, the temperatures at which 10 % and 50 % of the initial soot is converted ( $T_{10\%}$  and  $T_{50\%}$ , respectively) were

extracted from the CO<sub>x</sub> concentration curves. Figure 29 shows the plots of T<sub>10%</sub> (onset temperature) and T<sub>50%</sub> (half-conversion temperature) versus the catalyst/soot ratio.



**Figure 29. Temperature at which 10 % (T<sub>10%</sub>) and 50 % (T<sub>50%</sub>) of the initial soot is converted as a function of the catalyst/soot ratio.**

Both temperatures decrease with the catalyst/soot ratio. In particular, when moving from thermal regeneration (catalyst/soot ratio = 0) to almost purely catalytic regeneration (catalyst/soot ratio = 98 w/w), T<sub>10%</sub> decreases from ~525°C to ~350°C. Indeed, the onset temperature is more sensitive than the half-conversion temperature to variations in the catalyst/soot ratio and, thus, to variations in the soot-catalyst contact conditions. This trend

has also been found in catalytic combustion experiments with a ceria catalyst mixed in “loose” (with a spatula) and “tight” (in a mortar) contact with soot [Bueno-López, 2014].

In order to highlight the role of the ceria catalyst in soot oxidation, a temperature programmed regeneration test was carried out in the absence of gas-phase  $O_2$  and under conditions of good soot-catalyst contact (i.e., at catalyst/soot ratio equal to 125). In Figure 30, the  $CO_2$  and  $CO$  concentrations are plotted versus time along with the filter temperature.

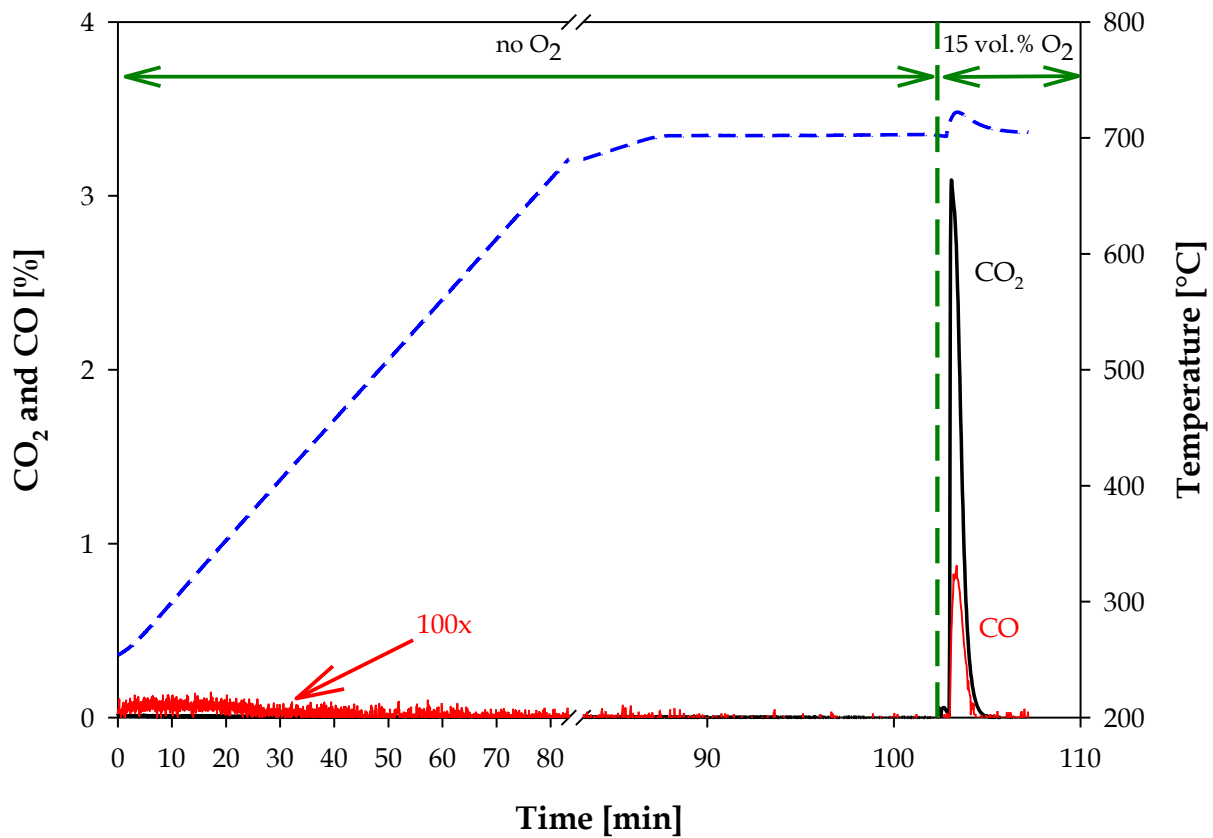


Figure 30.  $CO_2$  and  $CO$  concentrations and filter temperature versus time:

Temperature programmed regeneration test in the absence of gas-phase  $O_2$  at catalyst/soot ratio equal to 125.

In the absence of gas-phase  $O_2$ , no  $CO_x$  evolution is detected. Conversely, a rapid  $CO_x$  evolution is found when feeding  $O_2$ . These results clearly show that ceria activates gas-phase  $O_2$  to oxidize soot according to the “active oxygen” mechanism [Bueno-López, 2014].

## 7. Conclusions

In this work, the study of the regeneration of catalyst-coated diesel particulate filters was carried out.

Although widely investigated in literature, the contact taking place between the solid catalyst and soot has been generally studied by mixing more or less effectively the two powders, situation far from the real contact occurring in the structured filter.

On the other hand, attempts to use catalytic filters were made generally depositing a quite thin layer of catalyst on the filter walls. This condition dramatically reduces the filtration properties limiting the access of soot particles to the wall macropores interposing a solid layer with much smaller pores and, at the same time, strongly limited. In this thesis regeneration was studied reproducing on a lab-scale soot oxidation on a real catalytic filter. The work aimed at optimizing both catalyst dispersion on the filter and soot filtration condition to significantly reduce the combustion temperature approaching the almost totally catalytic oxidation.

The first results of this work was the suitable choice of catalyst particle size. The nano-sized CeO<sub>2</sub> used to washcoat the filter allowed a high dispersion with penetration of the catalyst into the filter walls without any detectable occlusion of macropores thus preserving the filtration properties. The right dosage of the catalyst, avoiding the formation of a thin layer hindering soot filtration represented another important result.

Finally, the link between regeneration performance and soot-catalyst distribution was identified and quantified.

Two different types of soot distribution were found:

- 1) at high catalyst/soot ratio ( $\sim 100$  w/w), the soot particles deeply penetrate into the macro-pores of the filter walls coming in close touch with ceria;
- 2) at low catalyst/soot ratio ( $\sim 20$  w/w), in addition to the soot particles trapped inside the macro-pores, a thick soot cake layer accumulates on top of the catalytic filter walls.

In going from condition 1) to condition 2), a transition occurs from an almost purely catalytic regeneration mode (with a large fraction of soot - around 80 % - burned via catalytic path) to a catalyst-assisted thermal regeneration mode (with around 80 % of soot burned via thermal path). This is a direct consequence of the increased cake thickness.

The results obtained in this work highlight the importance of strategies that avoid or minimize the segregation between the cake layer and the catalytic wall of the filter to operate catalyst-coated DPFs in an effective manner. Indeed, in spite of the considerable efforts made in the design of ceria-based soot combustion catalysts at laboratory, the main challenge still remains to increase the soot-ceria contact surface greatly on the filter.

A possible strategy for limiting the segregation between the soot and the catalyst, avoiding the formation of cake, could be represented by a continuous regeneration.

## **Acknowledgements**

This PhD Program was funded by the Institute for Research on Combustion (IRC) of the National Research Council (CNR) of Italy within the framework of the SOLYST project (FIRB - Futuro in Ricerca 2012 initiative of the Italian Ministry for Education, University and Research - MIUR, grant number: RBFR12LS6M 002).

## Literature Cited

- Ahlström, A.F., Odenbrand, C.U.I., Combustion of soot deposits from diesel engines on mixed oxides of vanadium pentoxide and cupric oxide, *Applied Catalysis* 60 (1990) 157-172.
- Aneghi, E., De Leitenburg, C., Dolcetti, G., Trovarelli, A., Promotional effect of surface Lanthanum in soot oxidation over ceria-based catalysts, *Topics in Catalysis* 42-43 (2007) 319-322.
- Aneghi, E., De Leitenburg, C., Trovarelli, A., On the role of lattice/surface oxygen in ceria-zirconia catalysts for diesel soot combustion, *Catalysis Today* 181 (2012) 108-115.
- Aneghi, E., Llorca, J., de Leitenburg, C., Dolcetti, G., Trovarelli, A., Soot combustion over silver-supported catalysts, *Applied Catalysis B* 91 (2009) 489-498.
- Atribak, I., Azambre, B., Bueno López, A., García-García A., Effect of NO<sub>x</sub> adsorption/desorption over ceria-zirconia catalysts on the catalytic combustion of model soot, *Applied Catalysis B* 92 (2009) 126-137.
- Badini, C., Saracco, G., Specchia, V., Combustion of carbon particulate catalysed by mixed potassium vanadates and KI, *Catalysis Letters* 55 (1998) 201-206.
- Bensaid, S., Marchisio, D., L., Fino, D., Numerical simulation of soot filtration and combustion within diesel particulate filters, *Chemical Engineering Science* 65 (2009) 357-363.

- Bensaïd, S. , Russo, N. , Fino, D., CeO<sub>2</sub> catalysts with fibrous morphology for soot oxidation: the importance of the soot-catalyst contact conditions, *Catalysis Today* 216 (2013) 57-63.
- Bueno-López, A., Diesel soot combustion ceria catalysts, *Applied Catalysis B: Environmental* 146 (2014) 1-11.
- Chen, K., Martirosyan, K.S., Luss, D., Counter-intuitive temperature excursions during regeneration of a diesel particulate filter, *AIChE Journal* 57 (2011b) 497-506.
- Chen, K., Martirosyan, K.S., Luss, D., Soot combustion dynamics in a planar diesel particulate filter, *Industrial & Engineering Chemistry Research* 48 (2009a) 3323-3330.
- Chen, K., Martirosyan, K.S., Luss, D., Temperature excursions during soot combustion in a diesel particulate filter (DPF), *Industrial & Engineering Chemistry Research* 49 (2010) 10358-10363.
- Chen, K., Martirosyan, K.S., Luss, D., Temperature gradients within a soot layer during DPF regeneration, *Chemical Engineering Science* 66 (2011a) 2968-2973.
- Chen, K., Martirosyan, K.S., Luss, D., Wrong-way behavior of soot combustion in a planar diesel particulate filter, *Industrial & Engineering Chemistry Research* 48 (2009b) 8451-8456.
- Ciambelli, P., Palma, V., Russo, P., Vaccaro, S., The effect of NO on Cu/V/K/Cl catalysed soot combustion, *Applied Catalysis B* 22 (1999) L5-L10.
- Cooper, B.J., Thoss, J.E., Role of NO in diesel particulate emission control, *SAE Technical Paper*, Paper Number 890404 (1989).

- Dettling, J.C., Skomoroski, R., Catalyzed diesel exhaust particulate filter, US Patent 5100632 A (Engelhard Corporation) (1992).
- DieselNet (2005), Diesel Filter Systems - Catalyzed Diesel Filters, in: DieselNet Technology Guide, [www.dieselnets.com](http://www.dieselnets.com).
- European Automotive Manufacturer's Association, European Union Economic Report, [www.acea.be](http://www.acea.be). (2010).
- Fino D., Russo N., Badini C., Saracco G., Specchia V., Effect of active species mobility on soot-combustion over Cs-V catalysts, *AIChE Journal* 49 (2003) 2173-2180.
- Fino, D., Diesel emission control: Catalytic filters for particulate removal, *Science and Technology of Advanced Materials* 8 (2007) 93-100.
- Fino, D., Specchia, V., Compositional and structural optimal design of a nanostructured diesel-soot combustion catalyst for a fast-regenerating trap, *Chemical Engineering Science* 59 (2004) 4825-4831.
- Fino, D., Specchia, V., Open issues in oxidative catalysis for diesel particulate abatement, *Powder Technology* 180 (2008) 64-73.
- Fino, D., Bensaid, S., Piumetti, M., Russo, N., A review on the catalytic combustion of soot in Diesel particulate filters for automotive applications: From powder catalysts to structured reactors, *Applied Catalysis A: General* 509 (2016) 75-96.
- Görsmann, C., Catalytic coatings for active and passive diesel particulate filter regeneration, *Monatshefte für Chemie* 136 (2005) 91-105.

- Guan, B., Zhan, R. , Lin, H., Huang, Z., Review of the state-of-the-art of exhaust particulate filter technology in internal combustion engines, *Journal of Environmental Management*, 154 (2015) 225-258.
- Hinot, K., Burtscher, H., Weber, A.P., Kasper, G., The effect of the contact between platinum and soot particles on the catalytic oxidation of soot deposits on a diesel particle filter, *Applied Catalysis B: Environmental* 71 (2007) 271-278.
- Johnson, J.H., Bagley, S.T., Gratz, L., Leddy, D., A review of diesel particulate control technology and emission effects, *SAE Technical Paper*, Paper Number 940233 (1994).
- Iojoiu, E.E., Bassou, B., Guilhaume, N., Farrusseng, D., Desmartin-Chomel, A., Lombaert, K., Bianchi, D., Mirodatos, C., High-throughput approach to the catalytic combustion of diesel soot, *Catalysis Today* 137 (2008) 103-109.
- Johnson, V.T., Diesel emission control in reviews the last 12 months, *SAE Technical Paper*, Paper Number 2003-01-0039 (2003).
- Kim, M.R., Kim, D.H., Woo, S.I., Effect of  $V_2O_5$  on the catalytic activity of Pt-based diesel oxidation catalyst, *Applied Catalysis B* 45 (2003) 269-279.
- Koltsakis, G.C., Haralampous, O.A., Samaras, Z.C., Kraemer, L., Heimlich, F., Behnk, K., Control Strategies for Peak Temperature Limitation in DPF Regeneration Supported by Validated Modeling, *SAE Technical Paper* 2007-01-1127 (2007).
- Konstandopoulos, A.G., Papaioannou, E., Update on the science and technology of diesel particulate filters, *KONA Powder and Particle Journal* 26 (2008) 36-65.

- Kumar, P.A. , Tanwar, M.D., Bensaid, S., Russo, N., Fino, D., Soot combustion improvement in diesel particulate filters catalyzed with ceria nanofibers, *Chemical Engineering Journal* 207-208 (2012) 258-266.
- Li, Z., Meng, M., Li, Q., Xie, Y., Hu, T., Zhang, J., Fe-substituted nanometric  $\text{La}_{0.9}\text{K}_{0.1}\text{Co}_{1-x}\text{Fe}_x\text{O}_{3-6}$  perovskite catalysts used for soot combustion,  $\text{NO}_x$  storage and simultaneous catalytic removal of soot and  $\text{NO}_x$ , *Chemical Engineering Journal* 164 (2010) 98-105.
- Liu, S., Obuchi, A., Oi-Uchisawa, J., Nanba, T., Kushiya, S., Synergistic catalysis of carbon black oxidation by Pt with  $\text{MoO}_3$  or  $\text{V}_2\text{O}_5$ , *Applied Catalysis B* 30 (2001) 259-265.
- Martirosyan, K.S., Chen, K., Luss, D., Behavior features of soot combustion in diesel particulate filter, *Chemical Engineering Science* 65 (2010) 42-46.
- Miceli, P., Bensaid, S., Russo, N., Fino, D., Effect of the morphological and surface properties of  $\text{CeO}_2$ -based catalysts on the soot oxidation activity, *Chemical Engineering Journal* 278 (2015) 190-198.
- Mul, G., Kapteijn, F., Moulijn, J.A., Catalytic oxidation of model soot by metal chlorides, *Applied Catalysis B* 12 (1997) 33-47.
- Neri, G., Bonaccorsi, L., Donato, A., Milone, C. , Musolino, M.G., Visco, A.M., Catalytic combustion of diesel soot over metal oxide catalysts, *Applied Catalysis B* 11 (1997) 217-231.
- Piumetti, M., Bensaid, S. , Russo, N., Fino, D., Nanostructured ceria-based catalysts for soot combustion: Investigations on the surface sensitivity., *Applied Catalysis B: Environmental* 165 (2015) 742-751.

- Prasad, R., Bella, V.R., A review on diesel soot emission, its effect and control, *Bulletin of Chemical Reaction Engineering & Catalysis* 5 (2010) 69-86.
- Querini, C.A., Ulla, M.A., Requejo, F., Soria, J., Sedrán, U.A., Miró, E.E., Catalytic combustion of diesel soot particles. Activity and characterization of Co/MgO and Co,K/MgO catalysts, *Applied Catalysis B* 15 (1998) 5-19.
- Rico Pérez, V., Bueno-López, A., Catalytic regeneration of Diesel Particulate Filters: Comparison of Pt and CePr active phases, *Chemical Engineering Journal* 279 (2015) 79-85.
- Rocco, V., Sistemi di filtrazione del particolato emesso da motori diesel, Università di Roma "Tor Vergata" - Dipartimento di Ingegneria Meccanica, [www.uniroma2.it/didattica/Motori/deposito/dispense\\_trap21.pdf](http://www.uniroma2.it/didattica/Motori/deposito/dispense_trap21.pdf) (2009).
- Satoh, N., Ohno, H., Nakatsuji, T., A NO<sub>x</sub> reduction system using ammonia storage-selective catalytic reduction in rich and lean operations, 15<sup>th</sup> Aachen Colloquium (Germany) 10-11 oct. 2006.
- Schmidt, N., Root, T., Wirojsakunchai, T., Schroeder, E., Kolodziej, C., Foster, D.E., Suga, T., Kawai, T., Detailed diesel exhaust particulate characterization and DPF regeneration behavior measurements for two different regeneration systems, SAE Technical Paper, Paper Number 2007-01-1063 (2007).
- Southward, B.W.L. , Basso, S., Pfeifer, M., SAE Technical Paper 2010-01-0558 (2010).
- Trovarelli, A., Fornasiero, P., Ceria-based Formulations in Catalysts for Diesel Soot Combustion, *Catalysis by Ceria and Related Materials*, second ed., Imperial College Press, London, 2013 (pp. 565-621).

- Uchisawa, J.O., Obuchi, A., Enomoto, R., Xu, J., Nanba, T., Liu, S., Kushiyama, S., Oxidation of carbon black over various Pt/MO<sub>x</sub>/SiC catalyst, *Applied Catalysis B* 32 (2001) 257-268.
- Uchisawa, J.O., Obuchi, A., Wang, S., Nanba, T., Ohi, A., Catalytic performance of Pt/MO<sub>x</sub> loaded over SiC-DPF for soot oxidation, *Applied Catalysis B* 43 (2003a) 117-129.
- Uchisawa, J.O., Obuchi, A., Zhao, Z., Kushiyama, S., Carbon oxidation with platinum supported catalysts, *Applied Catalysis B* 18 (1998) 183-187.
- Uchisawa, J.O., Wang, S., Nanba, T., Ohi, A., Obuchi, A., Improvement of Pt catalyst for soot oxidation using mixed oxide as a support, *Applied Catalysis B* 44 (2003b) 207-215.
- van Setten, B.A.A.L., Makkee, M., Moulijn J.A, Science and technology of catalytic diesel particulate filters, *Catalysis Reviews* 43 (2001) 489-564.
- van Setten, B.A.A.L., Russo, P., Jelles, S., J., Makkee, M., Ciambelli, P., Moulijn, J., A., Influence of NO<sub>x</sub> on soot combustion with supported molten salt catalysts, *Reaction Kinetics and Catalysis Letters* 67 (1999) 3-7.
- van Setten, B.A.A.L., Schouten, J., M., Makkee, M., Moulijn, J., A., Realistic contact for soot with an oxidation catalyst for laboratory studies, *Applied Catalysis B* 28 (2000) 253-257.
- Watabe, Y., Yamada, C., Irako, K., Murakami, Y., Use of a catalyst for cleaning exhaust gas particulates, *European Patent* 0092023 B1 (1986).
- Wojdyr, M., Fityk: a general-purpose peak fitting program, *Journal of Applied Crystallography* 43 (2010) 1126-1128.

- Yapaulo, R.A., Wirojsakunchai, E., Orita, T., Foster, D.E., Akard, M., Walker, L.R. , Lance, M.J., Impact of filtration velocities and particulate matter characteristics on diesel particulate filter wall loading, *International Journal of Engine Research* 10 (2009) 287-304.